Journal of Biomolecular Structure and Dynamics

ISSN: 0739-1102 (Print) 1538-0254 (Online) Journal homepage: www.tandfonline.com/journals/tbsd20

Novel beta-lactam substituted benzenesulfonamides: *in vitro* enzyme inhibition, cytotoxic activity and *in silico* interactions

Özcan Güleç, Cüneyt Türkeş, Mustafa Arslan, Yeliz Demir, Busra Dincer, Abdulilah Ece & Şükrü Beydemir

To cite this article: Özcan Güleç, Cüneyt Türkeş, Mustafa Arslan, Yeliz Demir, Busra Dincer, Abdulilah Ece & Şükrü Beydemir (2024) Novel beta-lactam substituted benzenesulfonamides: *in vitro* enzyme inhibition, cytotoxic activity and *in silico* interactions, Journal of Biomolecular Structure and Dynamics, 42:12, 6359-6377, DOI: 10.1080/07391102.2023.2240889

To link to this article: https://doi.org/10.1080/07391102.2023.2240889

JOURNAL OF BIOMOLECULAR STRUCTURE AND DYNAMICS
2024, VOL. 42, NO. 12, 6359–6377
https://doi.org/10.1080/07391102.2023.2240889

Novel beta-lactam substituted benzenesulfonamides: *in vitro* enzyme inhibition, cytotoxic activity and *in silico* interactions

Özcan Güleç[a], Cüneyt Türkeş[b], Mustafa Arslan[a], Yeliz Demir[c], Busra Dincer[d], Abdulilah Ece[e] and Şükrü Beydemir[f,g]

[a]Department of Chemistry, Faculty of Arts and Science, Sakarya University, Sakarya, Turkey; [b]Department of Biochemistry, Faculty of Pharmacy, Erzincan Binali Yıldırım University, Erzincan, Turkey; [c]Department of Pharmacy Services, Nihat Delibalta Göle Vocational High School, Ardahan University, Ardahan, Turkey; [d]Department of Pharmacology, Faculty of Pharmacy, Erzincan Binali Yıldırım University, Erzincan, Turkey; [e]Department of Pharmaceutical Chemistry, Faculty of Pharmacy, Biruni University, İstanbul, Turkey; [f]Department of Biochemistry, Faculty of Pharmacy, Anadolu University, Eskişehir, Turkey; [g]Bilecik Şeyh Edebali University, Bilecik, Turkey

Communicated by Ramaswamy H. Sarma

ABSTRACT

In this study, a library of twelve beta-lactam-substituted benzenesulfonamides (**5a–l**) was synthesized using the tail-approach method. The compounds were characterized using IR, ^{1}H NMR, ^{13}C NMR and elemental analysis techniques. These newly synthesized compounds were tested for their ability to inhibit the activity of two carbonic anhydrases (*h*CA) isoforms, I and II, and acetylcholinesterase (AChE) *in vitro*. The results showed that the synthesized compounds were potent inhibitors of *h*CA I, with K_Is in the low nanomolar range (66.60–278.40 nM) than the reference drug acetazolamide (AAZ), which had a K_I of 439.17 nM. The *h*CA II was potently inhibited by compounds **5a**, **5d–g** and **5l**, with K_Is of 69.56, 39.64, 79.63, 74.76, 78.93 and 74.94 nM, respectively (AAZ, K_I of 98.28 nM). Notably, compound **5a** selectively inhibited *h*CA II with a selectivity of $>$ 4-fold over *h*CA I. In terms of inhibition of AChE, the synthesized compounds had K_Is ranging from 30.95 to 154.50 nM, compared to the reference drug tacrine, which had a K_I of 159.61 nM. Compounds **5f**, **5h** and **5l** were also evaluated for their ability to inhibit the MCF-7 cancer cell line proliferation and were found to have promising anticancer activity, more potent than 5-fluorouracil and cisplatin. Molecular docking studies suggested that the sulfonamide moiety of these compounds fits snugly into the active sites of *h*CAs and interacts with the Zn^{2+} ion. Furthermore, molecular dynamics simulations were performed for 200 ns to assess the stability and dynamics of each enzyme-ligand complex. The acceptability of the compounds based on Lipinski's and Jorgensen's rules was also estimated from the ADME/T results. These results indicate that the synthesized molecules have the potential to be developed into effective and safe inhibitors of *h*CAs and AChE and could be lead agents.

ARTICLE HISTORY
Received 27 January 2023
Accepted 1 July 2023

KEYWORDS
Carbonic anhydrase; acetylcholinesterase; beta-lactam; MCF-7; *in silico* study

1. Introduction

Antibiotics are pharmaceuticals utilized to treat infections caused by bacteria in humans and animals. These agents exert their effects by either eradicating bacterial cells or inhibiting their growth and reproduction. Many antibiotics contain a beta-lactam ring in their chemical structure, characterized by a fused four-membered lactam ring, a free carboxylic acid group, and one or more substituted amino acid side chains (Osazee, 2016; Ramírez Granillo et al., 2015). Beta-lactams, a type of 2-azetidinone, are well-known heterocyclic compounds among organic and medicinal chemists. These compounds have a ring system that is a common structural feature of several broad-spectrum beta-lactam antibiotics, including penicillin, carbapenem, cephalosporin, monobactam, sulbactam, nocardicin and tazobactam, which are used as chemotherapeutic agents to treat microbial diseases (Mehta et al., 2010; Page, 1987; Singh, 2004a, 2004b).

Anticancer agents are critical for the control and elimination of cancer. However, the rapid emergence of resistance to most anticancer agents and the low specificity of these agents present significant challenges to effective cancer therapy. In recent years, there has been a significant effort to devise new chemotherapeutic strategies for the treatment of various types of cancer. Beta-lactam derivatives, in particular, have gained attention as a versatile pharmacophore for drug discovery due to their broad spectrum of pharmacological activity and their ability to induce DNA damage and apoptosis in various cancer cell lines. As such, beta-lactam derivatives are a promising and efficient platform for the development of new anticancer agents (Malebari et al., 2020; Veinberg et al., 2004; Zhang & Jia, 2020). Additionally, these

CONTACT Cüneyt Türkeş cuneyt.turkes@erzincan.edu.tr Department of Biochemistry, Faculty of Pharmacy, Erzincan Binali Yıldırım University, 24002 Erzincan, Turkey; Mustafa Arslan marslan@sakarya.edu.tr Department of Chemistry, Faculty of Arts and Sciences, Sakarya University, 54187 Sakarya, Turkey

This article has been corrected with minor changes. These changes do not impact the academic content of the article.

Supplemental data for this article can be accessed online at https://doi.org/10.1080/07391102.2023.2240889.

agents display a diverse range of biological activities such as anti-microbial (Kuskovsky et al., 2019), antibacterial (Carosso & Miller, 2015), antifungal (Wang et al., 2019), anti-hyperglycemic (Sahoo & Banik, 2020), anti-inflammatory (Saturnino et al., 2000), anti-HIV (Sperka et al., 2005), antimalarial (Rad et al., 2017), anti-tubercular (Kumar et al., 2012) and analgesic (Vigorita et al., 2001) activities. The biological activity of these compounds is often linked to the chemical reactivity of the lactam ring and the substituents, particularly at the nitrogen of the azetidinone ring (Brandi et al., 2008).

There are currently 15 different human carbonic anhydrase (*h*CA) isoenzymes that have been identified (Kakakhan et al., 2023; Leitans et al., 2015); they are found in many tissues and are involved in a wide range of metabolic processes (Alım et al., 2022; Ozer et al., 2022). With the highest turnover rate of all *h*CAs, *h*CA II is one of the most researched isoforms (k_{cat} of 10^6 s^{-1}) (Singh et al., 2019). The His64 residue, located near the active site, plays a role in rapid proton transfer, contributing to the high turnover rate of the enzyme (Fisher et al., 2007). The *h*CA II is in charge of controlling the intraocular pressure that typically accompanies glaucoma because it participates in the main transport pathway of sodium into the eye (Carta et al., 2012). One of the main reasons to investigate more closely at *h*CA II inhibitors was for the treatment of glaucoma, which if left untreated can result in blindness (Scozzafava & Supuran, 2014). In addition, the physiologically dominant isoform of the *h*CAs family (Table 1), *h*CA II, is expressed in a variety of brain cells and tissues (Topal, 2019), including oligodendrocytes (Taslimi et al., 2019), astrocytes (Daryadel et al., 2018), myelin sheaths (Supuran, 2018), choroid plexus (Mishra et al., 2021) and myelinated tracts (Mishra et al., 2017). Particularly, *h*CA II is overexpressed in many tumor types, and this overexpression has frequently been linked to the aggressiveness of tumor cells (Parkkila et al., 2010), as in the case of colorectal cancer (Bekku et al., 2000) and synchronous distant metastases (Lankat-Buttgereit et al., 2004).

The *h*CAs that are catalytically active contain a Zn^{2+} ion tetrahedrally coordinated by three histidine residues (His94, His96 and His119) (Aggarwal et al., 2013) and a water molecule at the base (Zhang et al., 1996). They also have a sizable active site split into two sides, one lined with hydrophobic residues and the other with polar, hydrophilic residues (Tawfik et al., 2022). Additionally, it is difficult to selectively inhibit one *h*CA isoform over others due to their catalytic regions' structural homology (Alterio et al., 2012) and amino acid sequence conservation (Mishra et al., 2020). The 'ring and tail' strategy is the most frequently utilized method to create *h*CA inhibitors (*h*CAIs) (Kumar et al., 2022). In this strategy, the 'ring' is made up of hetero/-aromatic fragments that contain a zinc-binding group (ZBG) (Eldeeb et al., 2021), which is necessary for binding zinc (Figure 1). The ability of electron acceptor substituents to make the ZBG more acidic and hence raise its acidity, makes them valuable (Bonardi et al., 2020). A flexible piece attached to the aromatic ring called the 'tail' plays a role in the compound's increased binding to the *h*CAs active site or enhances its solubility in water (Elbadawi et al., 2021). Unquestionably, sulfonamides, which play a significant role as zinc binders, are among the most productive and extensively researched derivatives for developing numerous isoform-selective and potent *h*CAIs, as well as in the associated therapeutic setting (Elbadawi et al., 2022).

At this instance, as part of our ongoing work on developing more potent and selective *h*CAIs, a novel combination of biologically active but structurally dissimilar groups, such as beta-lactam and sulfonamide, has been designed using the ring and tail approach. The structural characteristics of the newly synthesized beta-lactam substituted benzenesulfonamide derivatives (**5a–l**) with this approach were determined using various spectroscopic techniques (Scheme 1). Afterward, the cytosolic *h*CA isoforms I, II and AChE were tested for the target derivatives' inhibitory effects. In addition, the synthesized compounds were tested for their antiproliferative effects against the human breast cancer (MCF-7) cell line *in vitro*. Molecular docking studies of the target derivatives in *h*CAs and AChE were also conducted to examine the predicted *in silico* binding interactions of the novel synthesized derivatives with the active sites of these enzymes.

2. Materials and methods

2.1. General procedure for the preparation of the target compounds

The melting points of the compounds were determined using a Yanagimoto micro-melting point apparatus and were not corrected. Infrared spectra were obtained using a SHIMADZU Prestige-21 (200 VCE) spectrometer. Proton and carbon nuclear magnetic resonance spectra were acquired on a VARIAN Infinity Plus at 300 and 75 Hz, respectively,

Table 1. Organ or tissue distribution and subcellular localization of the *h*CAs.

*h*CAs	Organ or tissue distribution	Subcellular localization
I	Erythrocytes, eye, and gastrointestinal tract	Cytosol
II	Bone osteoclasts, brain, erythrocytes, eye, gastrointestinal tract, kidneys, lungs and testes	Cytosol
III	Adipocytes and skeletal muscles	Cytosol
IV	Brain capillaries, colon, eye, heart muscle, kidneys, lungs and pancreas	Membrane-bound
VA	Brain and liver	Mitochondria
VB	Gastrointestinal tract, heart or skeletal muscles, kidneys, pancreas and spinal cord	Mitochondria
VI	Salivary and mammary glands	Secreted
VII	Central nervous system	Cytosol
IX	Hypoxic tumors and gastrointestinal mucosa	Transmembrane
XII	Eye, hypoxic tumors, kidneys, and intestinal and reproductive epithelia	Transmembrane
XIII	Brain, gut, kidneys, lungs and reproductive tract	Cytosol
XIV	Brain, kidneys and liver	Transmembrane

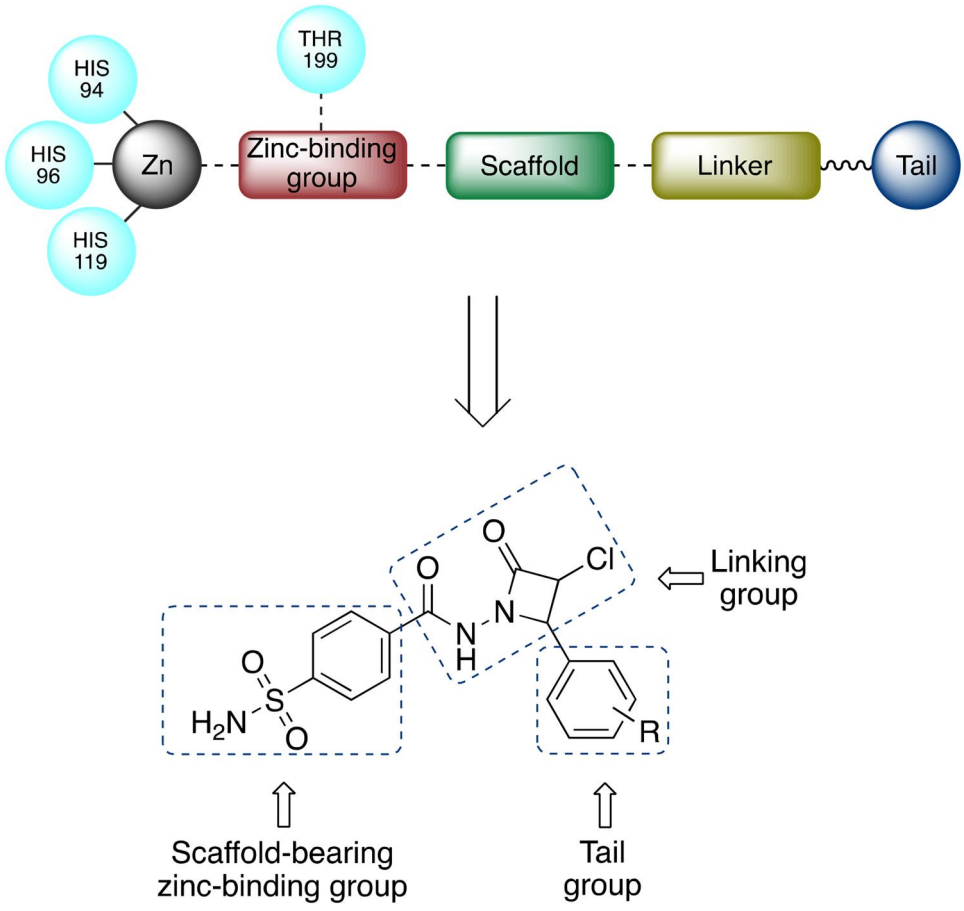

Figure 1. Illustration of the 'tail-approach' method and the synthesized target beta-lactam-substituted benzenesulfonamides **5a–l**.

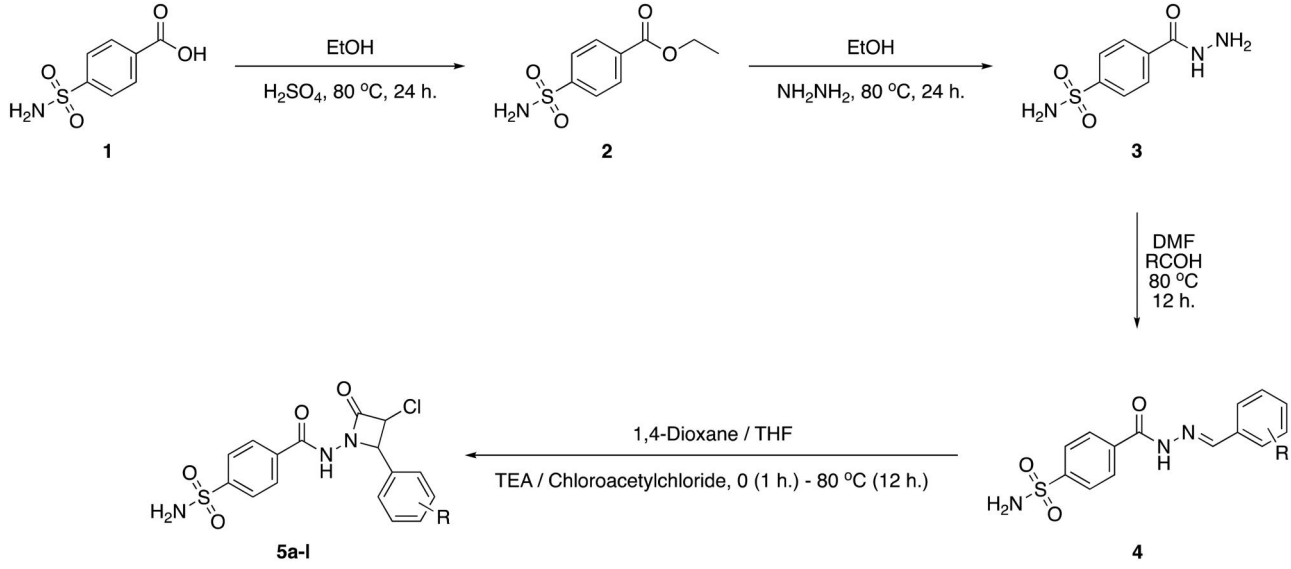

Compound ID	R	Compound ID	R	Compound ID	R
5a	4-H	5e	3-Br	5i	2-Cl,6-F
5b	4-CH_3	5f	4-Cl	5j	2-Cl,4-F
5c	4-OCH_3	5g	3-Cl	5k	4-CN
5d	4-Br	5h	4-F	5l	4-NO_2

Scheme 1. Synthetic pathway of target beta-lactam substituted benzenesulfonamides **5a–l**.

and the chemical shifts were referenced to the internal deuterated solvent. Elemental analysis was conducted using a Leco CHNS-932 instrument. All chemicals used in the study were purchased from Merck, Alfa Aesar, and Sigma-Aldrich.

2.2. General procedure for preparation of 4-sulfonylamide ester (2)

Sulfamoylbenzoic acid (10 mmol) was dissolved in 50 mL of ethanol and 1 mL of sulfuric acid and the mixture was refluxed for 24 h. The solvent was then removed by evaporation, and the resulting product was washed with cold water and dried. The product was characterized by NMR and used in the next step without further purification.

2.3. General procedure for preparation of 4-sulfonylamidebenzohydrazide (3)

The reaction of 4-sulfonylamide ester (10 mmol) and hydrazine hydrate (25 mmol) in ethanol was carried out by refluxing the mixture at 80 °C for 24 h. Upon cooling to room temperature, the solid product was obtained by filtering the reaction mixture, washing with water, and drying. The product was characterized by NMR spectroscopy and used in the next step without further purification.

2.4. Synthesis of (E)-4-(2-benzylidenehydrazinecarbonyl) benzenesulfonamide derivatives (4)

In the present study, the synthesis of benzaldehyde derivatives (2.5 mmol) through the reaction of 4-sulfonylamidebenzohydrazide (2.5 mmol) and DMF (10 mL) was carried out by refluxing the mixture at 80 °C for 12 h. Upon completion, the mixture was cooled and poured into ice-cold water before being filtered and crystallized from acetone. The resulting compounds were confirmed to have structural characteristics consistent with Schiff-base compounds based on ^{1}H and ^{13}C NMR spectra.

2.5. General procedure for preparation of targeted compounds (5a–l)

In this study, we synthesized and characterized a series of (*E*)-4-(2-benzylidenehydrazinecarbonyl)benzenesulfonamide derivatives (**4**) (1 mmol) through a reaction between 4-(2-benzylidenehydrazinecarbonyl)benzenesulfonamide (2.5 mmol) and chloroacetyl chloride (2.5 mmol). The reaction was carried out by dissolving the starting materials in a mixture of anhydrous 1,4-dioxane and THF, cooling the mixture to 0 °C, and adding chloroacetyl chloride. The mixture was stirred at 0 °C for 1 h, then refluxed at 80 °C for 12 h. After the reaction was complete, the mixture was cooled to room temperature, poured into ice-cold water, filtered, and crystallized from acetone. The resulting compounds were characterized using ^{1}H NMR, ^{13}C NMR, IR and elemental analysis. Also, the mass analysis was carried out with an LC–MS QTOF-9030 spectroscopy.

2.5.1. N-(3-Chloro-2-oxo-4-phenylazetydin-1-yl)-4-sulfamoylbenzamide (5a)

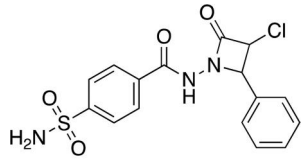

5a

Yield: 85%, m.p. 208 °C; ^{1}H NMR (300 MHz, DMSO-d_6, ppm): 8.05 (2H, d, =CH), 7.95 (2H, d, =CH), 7.28 (1H, s, –NH–), 7,64 (2H, s, NH_2), 7.43–7.61 (5H, m, =CH), 4.63 (1H, d, –CH), 4.77 (1H, d, –CH). ^{13}C NMR (75 MHz, DMSO-d_6, ppm): 163.4, 155.1, 147.6, 136.2, 130.9, 129.6, 128.1, 127.4, 127.2, 127.1, 93.4, 42.5. FT-IR (ν, cm^{-1}): 3289 (NH_2,), 3078 (=C–H), 1648 (C = O), 1340, 1159 (SO_2). Anal. Calcd. For $C_{16}H_{14}ClN_3O_4S$: C, 50.60; H, 3.72; Cl, 9.33; N, 11.06; O, 16.85; S, 8.44. Found: C, 50.57; H, 3.65; N, 11.02; O, 16.89; S, 8.46. QTOF LC–MS (*m/z* found: (M – H): 378.0304; calculated $[C_{16}H_{14}ClN_3O_4S]$: 378.0394 $[M-H]^-$.

2.5.2. N-(3-Chloro-2-oxo-4-(p-tolyl)azetydin-1-yl)-4-sulfamoylbenzamide (5b)

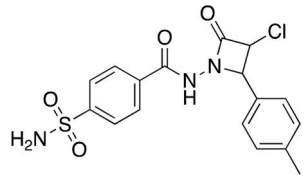

5b

Yield 72%, m.p 109 °C; ^{1}H NMR (300 MHz, DMSO-d_6, ppm): 8.11 (2H, d, =CH), 7.94 (2H, d, =CH), 7.56 (2H, s, –NH_2), 7.38 (2H, d, =CH), 7.20–7.25 (2H, d, =CH, 1H, s, NH), 4.62 (1H, d, –CH), 4.71 (1H, d, –CH), 2.54 (3H, s, –CH_3). ^{13}C NMR (75 MHz, DMSO-d_6, ppm): 163.1, 155.1, 147.6, 140.5, 133.3, 129.9, 129.4, 127.9, 127.2, 127.0, 93.3, 42.3, 21.6. FT-IR (ν, cm^{-1}): 3253 (NH_2), 3058 (=C–H), 1667 (C = O), 1350, 1162 (SO_2). Anal. Calcd. For $C_{17}H_{16}ClN_3O_4S$: C, 51.84; H, 4.10; Cl, 9.00; N, 10.67; O, 16.25; S, 8.14. Found: C, 51.80; H, 4.06; N, 10.61; O, 16.28; S, 8.12. QTOF LC–MS (*m/z* found: (M – H): 392.0460; calculated $[C_{17}H_{16}ClN_3O_4S]$: 392.0550 $[M-H]^-$.

2.5.3. N-(3-Chloro-2-(4-methoxyphenyl)-4-oxoazetydin-1-yl)-4-sulfamoylbenzamide (5c)

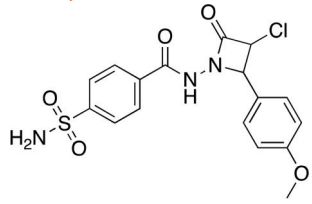

5c

Yield 81%, m.p. 127 °C. ^{1}H NMR (300 MHz, DMSO-d_6, ppm): 8.04 (2H, d, =CH), 7.92 (2H, d, =CH), 7.59 (2H, s, –NH_2), 7.43 (2H, d, =CH), 7.25 (1H, s, NH), 6.97 (2H, d, =CH), 4.60 (1H, d, –CH), 4.71 (1H, d, –CH), 3,79 (3H, s, –CH_3). ^{13}C NMR (75 MHz, DMSO-d_6, ppm): 163.0, 155.1, 147.5, 132.3, 128.9, 128.1, 127.9, 127.2, 126.3, 114.9, 93.3, 55.7, 42.2. FT-IR (ν, cm^{-1}): 3254 (NH_2,), 3038 (=C–H), 1659 (C = O), 1352, 1163

(SO_2). Anal. Calcd. For $C_8H_7N_3O_3S_2$: C, 37.35; H, 2.74; N, 16.33; O, 18.66; S, 24.93. Found: C, 37.24; H, 2.79; N, 16.32; O, 18.65; S, 24.83. QTOF LC–MS (*m/z* found: (M − H): 408.0042; calculated $[C_{17}H_{16}ClN_3O_5S]$: 408.0499 $[M-H]^-$.

2.5.4. N-(2-(4-Bromophenyl)-3-chloro-4-oxoazetydin-1-yl)-4-sulfamoylbenzamide (5d)

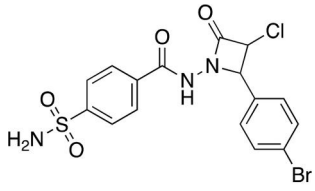

5d

Yield 78%, m.p. 105 °C; ^{1}H NMR (300 MHz, DMSO-d_6, ppm): 8.12 (2H, d, =CH), 7.96 (2H, d, =CH), 7.72 (2H, d, =CH), 7.60 (2H, s, –NH_2), 7.54 (2H, d, =CH), 7.29 (1H, s, NH), 4,79 (1H, d, –CH), 4,62 (1H, d, –CH). ^{13}C NMR (75 MHz, DMSO-d_6, ppm): 163.5, 155.2, 147.6, 135.5, 132.6, 129.7, 128.2, 127.1, 124.4, 92.7, 42.5. FT-IR (ν, cm^{-1}): 3259 (NH_2), 3078 (=C–H), 1668 (C = O), 1349, 1160 (SO_2). Anal. Calcd. For $C_{16}H_{13}BrClN_3O_4S$: C, 41.89; H, 2.86; Br, 17.42; Cl, 7.73; N, 9.16; O, 13.95; S, 6.99. Found: C, 41.87; H, 2.84; N, 9.11; O, 13.99; S, 6.94. QTOF LC–MS (*m/z* found: (M − H): 455.9419; calculated $[C_{16}H_{13}BrClN_3O_4S]$: 455.9499 $[M-H]^-$.

2.5.5. N-(2-(3-Bromophenyl)-3-chloro-4-oxoazetidin-1-yl)-4-sulfamoylbenzamide (5e)

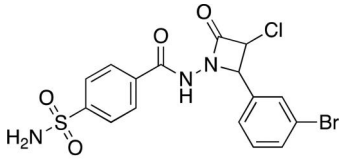

5e

Yield 65%, m.p. 94 °C; ^{1}H NMR (300 MHz, DMSO-d_6, ppm): 8.08 (2H, d, =CH), 7.94 (2H, d, =CH), 7.75 (1H, s, =CH), 7.68 (1H, d, =CH), 7.58 (2H, s, –NH_2), 7.56 (1H, d, =CH), 7.46 (1H, t, =CH), 7.32 (1H, s, NH), 4.79 (1H, d, –CH), 4.66 (1H, d, –CH). ^{13}C NMR (75 MHz, DMSO-d_6, ppm): 163.6, 155.1, 147.6, 138.6, 133.8, 131.8, 130.3, 128.2, 127.1, 126.5, 122.7, 92.4, 42.6. FT-IR (ν, cm^{-1}): 3256 (NH_2), 3071 (=C–H), 1671 (C = O), 1345, 1155 (SO_2). Anal. Calcd. For $C_{16}H_{13}BrClN_3O_4S$: C, 41.89; H, 2.86; Br, 17.42; Cl, 7.73; N, 9.16; O, 13.95; S, 6.99. Found: C, 41.84; H, 2.81; N, 9.11; O, 13.92; S, 6.91. QTOF LC–MS (*m/z* found: (M − H): 455.9419; calculated $[C_{16}H_{13}BrClN_3O_4S]$: 455.9499 $[M-H]^-$.

2.5.6. N-(3-Chloro-2-(4-chlorophenyl)-4-oxoazetidin-1-yl)-4-sulfamoylbenzamide (5f)

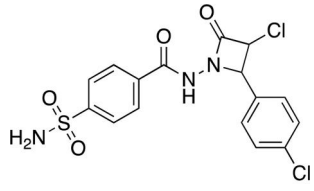

5f

Yield 74%, m.p. 194 °C; ^{1}H NMR (300 MHz, DMSO-d_6, ppm): 8.11 (2H, d, =CH), 7.98 (2H, d, =CH), 7.42–7.68 (4H, m, =CH), (2H, m, –NH_2), 7.32 (1H, s, NH), 4,76 (1H, d, –CH), 4,63 (1H, d, –CH). ^{13}C NMR (75 MHz, DMSO-d_6, ppm): 163.5, 155.1, 147.6, 135.6, 135.2, 129.7, 129.4, 128.2, 127.1, 126.5, 92.4, 42.5. FT-IR (ν, cm^{-1}): 3298 (NH_2), 3068 (=C–H), 1648 (C = O), 1351, 1158 (SO_2). Anal. Calcd. For $C_{16}H_{13}Cl_2N_3O_4S$: C, 46.39; H, 3.16; Cl, 17.11; N, 10.14; O, 15.45; S, 7.74. Found: C, 46.33; H, 3.12; Cl, 17.06; N, 10.18; O, 15.41; S, 7.65. QTOF LC–MS (*m/z* found: (M − H): 411.9919; calculated $[C_{16}H_{13}Cl_2N_3O_4S]$: 412.0004 $[M-H]^-$.

2.5.7. N-(3-Chloro-2-(3-chlorophenyl)-4-oxoazetidin-1-yl)-4-sulfamoylbenzamide (5 g)

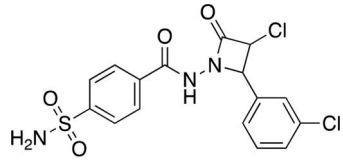

5g

Yield 80%, m.p. 107 °C; ^{1}H NMR (300 MHz, DMSO-d_6, ppm): 8.12 (2H, d, =CH), 7,95 (2H, d, =CH), 7,44–7,67 (6H, m, =CH & –NH_2), 7.28 (1H, s, NH), 4.78 (1H, d, CH), 4.65 (1H, d, CH). ^{13}C NMR (75 MHz, DMSO-d_6, ppm): 163.6, 155.1, 147.6, 138.4, 134.2, 131.6, 130.9, 128.2, 127.5, 127.1, 126.2, 92.4, 42.6. FT-IR (ν, cm^{-1}): 3270 (NH_2), 3048 (=C–H), 1669 (C = O), 1355, 1157 (SO_2). Anal. Calcd. For $C_{16}H_{13}Cl_2N_3O_4S$: C, 46.39; H, 3.16; Cl, 17.11; N, 10.14; O, 15.45; S, 7.74. Found: C, 46.35; H, 3.13; Cl, 17.04; N, 10.11; O, 15.38; S, 7.69. QTOF LC–MS (*m/z* found: (M − H): 411.9918; calculated $[C_{16}H_{13}Cl_2N_3O_4S]$: 412.0004 $[M-H]^-$.

2.5.8. N-(3-Chloro-2-(4-fluorophenyl)-4-oxoazetidin-1-yl)-4-sulfamoylbenzamide (5h)

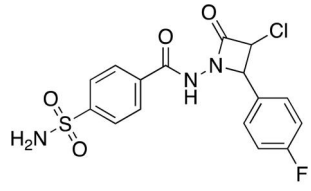

5h

Yield 82%, m.p. 207 °C; ^{1}H NMR (300 MHz, DMSO-d_6, ppm): 8.05 (2H, d, =CH), 7.92, (2H, d, =CH), 7.49–7,65 (4H, m, =CH & –NH_2), 7.21–7.32 (3H, m, =CH & –NH), 4.75 (1H, d, CH), 4.62 (1H, d, CH). ^{13}C NMR (75 MHz, DMSO-d_6, ppm): 163.2, 155.2, 132.2, 129.6, 127.8, 127.0, 126.9, 116.4, 116.2, 92.6, 42.2. FT-IR (ν, cm^{-1}): 3299 (NH_2), 3076 (=C–H), 1645 (C = O), 1345, 1157 (SO_2). Anal. Calcd. For $C_{16}H_{13}ClFN_3O_4S$: C, 48.31; H, 3.29; Cl, 8.91; F, 4.78; N, 10.56; O, 16.09; S, 8.06. Found: C, 48.28; H, 3.33; N, 10.47; O, 16.13; S, 8.01. QTOF LC–MS (*m/z* found: (M − H): 396.0213; calculated $[C_{16}H_{13}FClN_3O_4S]$: 396.0299 $[M-H]^-$.

2.5.9. N-(3-Chloro-2-(2-chloro-6-fluorophenyl)-4-oxoazetidin-1-yl)-4-sulfamoylbenzamide (5i)

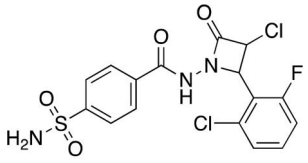

5i

Yield 84%, m.p. 108 °C; ^{1}H NMR (300 MHz, DMSO-d_6, ppm): 8.05 (2H, d, =CH), 7.93 (2H, d, =CH), 7.49–7.63 (4H, m, =CH, NH & –NH_2), 7.44 (1H, d, =CH), 7.34 (1H, t, =CH), 4.68 (1H, d, CH), 4.57 (1H, d, CH). ^{13}C NMR (75 MHz, DMSO-d_6, ppm): 162.8, 155.0, 147.6, 134.6, 133.5, 133.4, 127.8, 126.9, 120.7, 116.0, 87.8, 42.0. FT-IR (ν, cm^{-1}): 3237 (NH_2), 3053 (=C–H), 1664 (C = O), 1350, 1153 (SO_2). Anal. Calcd. For $C_{16}H_{12}Cl_2FN_3O_4S$: C, 44.46; H, 2.80; Cl, 16.40; F, 4.40; N, 9.72; O, 14.81; S, 7.42. Found: C, 44.42; H, 2.85; N, 9.69; O, 14.78; S, 7.37. QTOF LC–MS (*m/z* found: (M – H): 429.9822; calculated $[C_{16}H_{12}Cl_2FN_3O_4S]$: 429.9830 $[M-H]^-$.

2.5.10. N-(3-Chloro-2-(2-chloro-4-fluorophenyl)-4-oxoazetidin-1-yl)-4-sulfamoylbenzamide (5j)

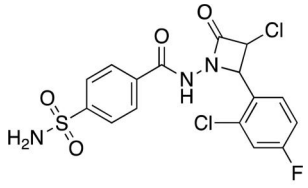

5j

Yield 70%, m.p. 125 °C; ^{1}H NMR (300 MHz, DMSO-d_6, ppm): 8.0 (2H, d, =CH), 7,94 (2H, d, =CH), 7.49–7.68 (4H, m, =CH & –NH_2), 7.44 (1H, s, –NH), 7,34 (1H, t, =CH), 4.78 (1H, d, CH), 4.62 (1H, d, CH). ^{13}C NMR (75 MHz, DMSO-d6, ppm): 163.4, 155.0, 147.6, 134.4, 134.3, 131.9, 131.8, 129.0, 127.8, 126.9, 118.4, 115.7, 91.0, 42.2. FT-IR (ν, cm^{-1}): 3246 (NH_2), 3053 (=C–H), 1664 (C = O), 1345, 1153 (SO_2). Anal. Calcd. For $C_{16}H_{12}Cl_2FN_3O_4S$: C, 44.46; H, 2.80; Cl, 16.40; F, 4.40; N, 9.72; O, 14.81; S, 7.42. Found: C, 44.38; H, 2.75; N, 9.68; O, 14.79; S, 7.34. QTOF LC–MS (*m/z* found: (M – H): 429.9927; calculated $[C_{16}H_{12}Cl_2FN_3O_4S]$: 429.9830 $[M-H]^-$.

2.5.11. N-(3-Chloro-2-(4-cyanophenyl)-4-oxoazetidin-1-yl)-4-sulfamoylbenzamide (5k)

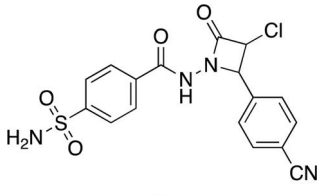

5k

Yield 76%, m.p. 98 °C; ^{1}H NMR (300 MHz, DMSO-d_6, ppm): 8.09–7.96 (6H, m, =CH), 7.78 (2H, d, =CH), 7.58 (2H, s, –NH_2), 7.38 (1H, s, –NH), 4.77 (1H, d, CH), 4.63 (1H, d, CH). ^{13}C NMR (75 MHz, DMSO-d_6, ppm): 163.5, 155.2, 147.7, 140.6, 133.3, 128.3, 118.6, 113.8, 92.2, 42.2. FT-IR (ν, cm^{-1}): 3237 (NH_2), 3057 (=C–H), 2228 (CN), 1669 (C = O), 1352, 1157 (SO_2). Anal. Calcd. For $C_{17}H_{13}ClN_4O_4S$: C, 50.44; H, 3.24; Cl, 8.76; N, 13.84; O, 15.81; S, 7.92. Found: C, 50.41; H, 3.29; N, 13.77; O, 15.76; S, 7.84. QTOF LC–MS (*m/z* found: (M – H): 403.0261; calculated $[C_{17}H_{13}ClN_4O_4S]$: 403.0346 $[M-H]^-$.

2.5.12. N-(3-Chloro-2-(4-nitrophenyl)-4-oxoazetidin-1-yl)-4-sulfamoylbenzamide (5 l)

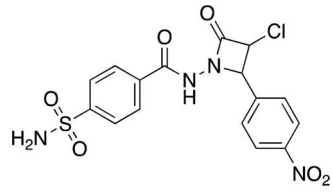

5l

Yield 80%, m.p. 102 °C; ^{1}H NMR (300 MHz, DMSO-d_6, ppm): 8.34 (2H, d, =CH), 8.10 (2H, d, =CH), 7.98 (2H, d, =CH), 7.82 (2H, d, =CH), 7.58 (2H, s, –NH_2), 7.0 (1H, s, NH), 4.78 (1H, d, CH), 4.61 (1H, d, CH). ^{13}C NMR (75 MHz, DMSO-d_6, ppm): 163.6, 155.3, 149.0, 147.7, 142.2, 130.3, 129.0, 128.7, 127.9, 126.9, 126.7, 125.9, 124.4, 91.8, 42.2. FT-IR (ν, cm^{-1}): 3232 (NH_2), 3043 (=C–H), 1679 (C = O), 1344, 1157 (SO_2). Anal. Calcd. For $C_{16}H_{13}ClN_4O_6S$: C, 45.24; H, 3.08; Cl, 8.34; N, 13.19; O, 22.60; S, 7.55. Found: C, 45.27; H, 3.013; N, 13.14; O, 22.53; S, 7.52. QTOF LC–MS (m/z found: (M – H): 423.0161; calculated $[C_{16}H_{13}ClN_4O_6S]$: 423.0244 $[M-H]^-$.

2.6. hCA and AChE inhibitory effect study

The human erythrocyte *h*CA I and II isoforms were isolated using Sepharose-4B-L-tyrosine-sulfanilamide affinity chromatography. The esterase activity of the *h*CAs was measured using Verpoorte's method (Verpoorte et al., 1967; Yararli et al., 2023), which involves the assessment of the change in absorbance at 348 nm, in order to determine the inhibitory effects of the newly synthesized beta-lactam substituted benzenesulfonamides (**5a–l**). The activity of *h*CAs was measured at 25 °C using the same substrate, 4-nitrophenyl acetate (PubChem CID: 13244) as in our earlier tests (Askin et al., 2021; Güleç et al., 2022; Lolak et al., 2022; Osmaniye et al., 2022; Türkeş et al., 2019). The reaction mix (approx. 1 mL) consisted of substrate (3 mM), *h*CA, and Tris-sulfate buffer (50 mM, pH 7.4). The enzyme unit was calculated using the absorption coefficient ($\varepsilon = 5.4 \times 10^3$ M^{-1} cm^{-1}) (Karakılıç et al., 2022). Additionally, using Ellman's method (Ellman et al., 1961), spectrophotometric measurements at room temperature were conducted to determine the effects of these novel synthesized derivatives on AChE (Sigma C2888, Type V-S) activity (Yakan et al., 2023). As in our earlier research, the results were achieved using the substrate acetylthiocholine iodide (AChI, Sigma 01480, PubChem CID: 74629) (Demir et al., 2023; Güller et al., 2021). The reaction mixture contained 10 mM of AChI and 0.5 mM 5,5′-dithiobis(2-nitrobenzoic acid) in 1 mM Tris/HCl (pH 8.0) containing 5 mM EDTA. The assay for AChE activity was based on the reaction of DTNB ($\varepsilon = 13.6\,M^{-1}\,cm^{-1}$) at 412 nm (Atmaca et al., 2022; Gök et al., 2021). These compounds (**5a–l**), as well as the reference medications AAZ and THA, were initially dissolved in

Table 2. Active binding sites of 1AZM, 3HS4, and 7E3I. To accept the effective binding of the compounds, site analysis by the SiteMap tool has a significant role in molecular docking studies. For this purpose, the essential binding site was selected according to the site score from among the five active sites.

Protein		SiteScore	Size[a]	Dscore[b]	Volume[c]	Exposure[d]	Enclosure[d]	Contact[e]	Phobic[f]	Philic[f]	Balance[f]	Don/Acc[g]
1AZM	Site 1	0.864	69	0.833	197.911	0.589	0.681	0.903	0.509	1.094	0.465	0.908
	Site 2	0.739	48	0.518	97.412	0.586	0.645	0.962	0.000	1.596	0.000	0.483
	Site 3	0.647	37	0.518	77.175	0.689	0.600	0.830	0.087	1.269	0.069	0.346
	Site 4	0.546	24	0.468	62.426	0.774	0.578	0.735	0.247	1.042	0.237	0.927
	Site 5	0.513	19	0.440	43.218	0.716	0.555	0.798	0.070	0.928	0.076	0.675
3HS4	Site 1	0.790	62	0.645	128.625	0.656	0.618	0.854	0.043	1.429	0.030	1.180
	Site 2	0.721	50	0.706	161.210	0.758	0.565	0.728	0.199	0.913	0.218	1.093
	Site 3	0.686	42	0.584	103.586	0.628	0.615	0.869	0.102	1.209	0.084	0.834
	Site 4	0.660	35	0.543	56.595	0.573	0.638	1.048	0.546	1.216	0.449	0.729
	Site 5	0.513	23	0.436	48.706	0.742	0.540	0.678	0.114	1.037	0.110	0.824
7E3I	Site 1	1.087	200	1.100	406.112	0.465	0.823	1.062	0.808	1.023	0.790	0.604
	Site 2	1.077	112	1.026	215.404	0.367	0.813	1.126	0.786	1.233	0.638	0.573
	Site 3	1.059	117	1.003	219.520	0.384	0.786	1.066	0.791	1.254	0.631	0.444
	Site 4	1.028	105	1.018	357.749	0.602	0.740	0.918	0.468	1.122	0.417	0.733
	Site 5	0.997	267	1.003	843.437	0.644	0.694	0.882	0.294	1.082	0.272	0.785

[a]Site size.
[b]Druggability score.
[c]Site volume.
[d]Exposure and enclosure, these two properties provide different measures of how open the site is to solvent.
[e]Contact, the contact property measures how strongly the average site point interacts with the surrounding receptor *via* van der Waals nonbonded interactions, when the site point is given nominal van der Waals parameters. The contact score has been calibrated so that the average score for a tight-binding site is 1.0.
[f]Hydrophobic and hydrophilic character, and balance, these properties, labeled phob and phil, measure the site's relative hydrophobic and hydrophilic character.
[g]Donor/acceptor character, this property, labeled don/acc, indicates the degree to which a well-structured ligand might be expected to donate, rather than accept, hydrogen bonds, as inferred from the sizes and intensities of donor and acceptor SiteMap regions.

DMSO at a concentration of 1 mg/mL. DMSO was present in the final reaction mixture at a concentration of around 1%. Each sample underwent three measurements. V_{max}, K_m and K_I values, and inhibition types for beta-lactam substituted benzenesulfonamide compounds **5a–l** were calculated from the data acquired by Michaelis–Menten (Michaelis et al., 2011) and Lineweaver–Burk (Kim et al., 2007) plots as in our earlier research (Yapar et al., 2021). The analysis of data and creation of graphs were carried out using GraphPad Prism V9 (GraphPad Software, La Jolla California USA) for Mac. The inhibition constants were calculated using SigmaPlot V12 (Systat Software, San Jose, CA, USA) for Windows. Statistical comparisons between data sets were performed using the extra sum-of-squares *F* test and the Akaike information criterion approach, and results are presented as mean ± standard error of the mean (95% confidence intervals). Statistical significance was determined when the *p*-value was less than 0.05.

2.7. Cytotoxic activity study

The human breast cancer (MCF-7) cell line was thawed and cultured in a 75 cm^2 flask with DMEM and 10% FBS. After 48 h, the cells were transferred to a 96-well plate and incubated at 37 °C in a 5% CO_2 atmosphere. The cells were then exposed to various concentrations (1–100 μM) of compounds **5d**, **5f**–**i** and **5l** for 24 h. The cytotoxic effects of these compounds were then evaluated using the MTT assay (Buza et al., 2023). Specifically, 10 μL of MTT solution (5 mg/mL) was added to each well, and the plate was incubated for an additional 3 h in a 5% CO_2 atmosphere. The absorbance of the formazan crystals formed as a result of the MTT assay was then measured at 570 nm using an Epoch Microplate Spectrophotometer. The cell viability rates were calculated by comparing the absorbance of the treated cells to that of the untreated control cells and expressed as a percentage. The IC_{50} values were determined using GraphPad Prism V9 (GraphPad Software, La Jolla, CA, USA) for Mac.

2.8. In silico study

In this study, we used the Small-Molecule Drug Discovery Suite 2023-1 for Mac (Schrödinger, LLC, NY, USA) to perform molecular docking analysis. The *h*CA I (PDB ID 1AZM, A chain, 2.00 Å) (Chakravarty & Kannan, 1994), *h*CA II (PDB ID 3HS4, A chain, 1.10 Å) (Sippel et al., 2009), and AChE (PDB ID 7E3I, A chain, 2.85 Å) (Cheung et al., 2012) protein structures were obtained from the RCSB Protein Data Bank (https://www.rcsb.org) and prepared for docking using the Protein Preparation Wizard (Madhavi Sastry et al., 2013; Schrödinger release 2023-1: Protein preparation wizard, 2023). The beta-lactam substituted benzenesulfonamides (**5a–l**) were drawn using ChemDraw V21.0 (PerkinElmer, Inc., Waltham, MA, USA) for Mac (Sever et al., 2021) and optimized in the OPLS4 force field with Epik (Schrödinger release 2023-1: Epik, 2023; Shelley et al., 2007) using the LigPrep module (Schrödinger release 2023-1: LigPrep, 2023) at pH 7.4 ± 0.5. The active site residues of the proteins were identified using the SiteMap tool (Halgren, 2009) and defined in the Receptor Grid Generation module to create the receptor grid in the Maestro panel (Schrödinger release 2023-1: Receptor grid generation, 2023; Yararli et al., 2023). The SiteMap tool (Schrödinger release 2023-1: SiteMap, 2023) determines one or more regions on or near the protein surface, called sites, and particularly calculates SiteScore, which has proven effective at identifying known binding sites in co-crystallized complexes. Here, the site of binding of the compounds was determined as Site 1, which had the best SiteScore (0.864, 0.790 and 1.087 for 1AZM, 3HS4 and 7E3I, respectively) among five suitable active sites (Table 2). The Glide application with the enhanced precision (XP) approach (Ece, 2020; Friesner et al., 2004; Halgren et al., 2004; Schrödinger release

2023-1: Glide, 2023) was used to dock the ligands to *h*CAs and AChE with default settings (Türkeş et al., 2021). The relative binding affinity of the protein-ligand complexes was predicted using the MM-GBSA approach (Barreiro et al., 2007; Schrödinger release 2023-1: Prime, 2023) in the VSGB energy model and OPLS4 force field.

Molecular dynamics (MD) simulations were performed using Desmond (Bowers et al., 2006) package implemented in Schrödinger software (Schrödinger release 2023-1: Desmond, 2023). The input protein and ligand complexes were obtained from docking studies. The system was solvated with the transferable intermolecular potential with three points (TIP3P) model in an orthorhombic simulation box. Sodium counterions were placed to neutralize the systems. Moreover, the physiological conditions were mimicked by adding 0.15 M NaCl. Normal pressure (1.01325 bar) and temperature (300 K) (NPT) ensemble were used in MD simulations. All equilibrated systems were first relaxed and then subjected to an MD run for 200 ns with a recording interval of 200 ps that generated approximately 1000 frames. Simulation Interaction Diagram (SID) tool to analyze MD results involving the root-mean-square deviation (RMSD), root-mean-square fluctuation (RMSF), and protein–ligand contacts.

ADME/T (absorption, distribution, metabolism, elimination and toxicity) properties such as central nervous system activity (CNS), molecular weight (MW), computed dipole moment (Dipole), total solvent-accessible volume (Volume), the estimated number of donor hydrogen bonds (donorHB), the estimated number of accepted hydrogen bonds (accptHB), octanol/gas partition coefficient (QPlogPoct), water/gas partition coefficient (QPlogPw), octanol/water partition coefficient (QPlogPo/w), aqueous solubility (QPlogS), apparent Caco-2 cell permeability (QPPCaco), brain/blood partition coefficient (QPlogBB), skin permeability (QPlogKp), number of likely metabolic reactions (Metab), prediction of binding to human serum albumin (QPlogKhsa), human oral absorption (HOA) and van der Waals surface area of polar nitrogen and oxygen atoms (PSA) for all compounds (**5a–l**) were predicted using the QikProp program (Güngör et al., 2022; Schrödinger release 2023-1: QikProp, 2023).

3. Results and discussion

3.1. Drug design strategy and chemistry

The ring and tail strategy has emerged as an effective approach due to the shared similarities in the active sites of *h*CAs (Bozdag et al., 2014). This method targets specific hydrophobic or hydrophilic residues in the outer region of the isoform active site by introducing various aryl or heterocyclic scaffolds to the aromatic sulfonamide ring of *h*CAIs (Nocentini & Supuran, 2019). The target derivatives (**5a–l**) in this study have a benzenesulfonamide-based ZBG attached to a beta-lactam scaffold. The beta-lactam moiety increases the flexibility and hydrophilicity of the designed compounds through advantageous interactions with specific residues in the hydrophilic region of the active site, enabling selective inhibition of *h*CA II. The hydrophobic tail is constructed using the phenyl moiety, which is connected to the hydrophobic or hydrophilic rims of the active site through the scaffold, ensuring proper orientation.

Ethyl 4-(aminosulfonyl)benzoate was synthesized from sulfamoylbenzoic acid in ethanol with a catalytic amount of sulfuric acid, with the reaction being carried out under reflux for 24 h. The ester group of ethyl 4-(aminosulfonyl)benzoate was then converted to the 4-sulfonylamidebenzohydrazide compound using hydrazine hydrate in ethanol at 80 °C for 24 h. The aldehyde derivatives and 4-sulfonylamidebenzohydrazide were dissolved in DMF and stirred at 80 °C for 24 h to form the synthesized imine derivatives. These derivatives were then dissolved in a mixture of dry dioxane-THF in the presence of a TEA base in an ice bath, and chloroacetylchloride was slowly added. The mixture was refluxed for 12 h to yield the prepared compounds (**5a–l**) shown in Scheme 1.

These compounds were characterized by ^{1}H NMR, ^{13}C NMR, IR, and elemental analysis. The ^{1}H NMR spectra of the compounds showed NH_2 and =CH proton peaks on the aromatic ring at around 7.50–7.60 and 8.00–8.30 ppm, respectively. The amide NH peak resonances were observed between 7.20 and 7.40 ppm (Arya et al., 2013). Hydrogen atoms on the lactam ring appeared as a doublet at around 4.75 ppm. The lactam ring and amide carbonyl carbon signals were seen at around 165 ppm and 155 ppm, respectively, in the ^{13}C NMR spectra. The infrared spectra of compounds **5a-l** displayed absorptions around 3250 cm^{-1} and 1670 cm^{-1} corresponding to N–H and C=O stretchings, respectively. Two peaks were assigned to SO_2 stretching, appearing at around 1300 cm^{-1} and 1100 cm^{-1} as asymmetric and symmetric stretches, respectively (Kılıcaslan et al., 2016). All spectra data support the structure of the synthesized compounds.

3.2. hCA and AChE inhibitory effect of the target compounds

The inhibitory effects of newly synthesized beta-lactam substituted benzenesulfonamide derivatives (**5a–l**) were examined against *h*CA I, II isoforms, and AChE. Acetazolamide (AAZ, PubChem CID: 1986) and tacrine (THA, PubChem CID: 1935) were included as standard inhibitors in the experiments. The inhibitory effect of these pharmacophores on the *h*CA II isoform was found to be significantly impacted by the diversity of substituents. The structure-activity relationship (SAR) was determined using enzyme inhibition constants (K_I) and coefficients of determination (R^2) and is presented in Table 3.

The cytosolic isoform *h*CA I was potently inhibited by herein reported novel synthesized beta-lactam substituted benzenesulfonamide derivatives with K_Is in the low nanomolar range of 66.60–278.40 nM, indicating that all synthesized molecules (**5a–l**) are higher selective and more potent inhibitors than reference drug AAZ (K_I of 439.17 nM). The most active derivatives in this series enclose 4-fluoro **5h**, 4-nitro **5 l**, and 4-bromo **5d** groups, which have K_Is of 66.60, 68.63 and 85.53 nM, respectively. The 3-bromo **5e**, 4-cyano **5k**, and unsubstituted **5a** derivatives (K_Is of 202.00, 260.50 and

Table 3. The inhibitory effects of the novel beta-lactam substituted benzenesulfonamides **5a–l** on cytosolic human CA isoforms *h*CA I, II, and AChE.

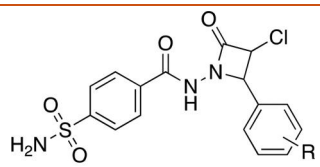

5a-l

Compounds		*h*CA I[a]		*h*CA II[b]		AChE[c]		S_I[d]	
ID	R	K_I (nM)	R^2	II/I	R^2	K_I (nM)	R^2	I/II	II/I
5a	4-H	278.40 ± 38.97	0.9748	69.56 ± 14.77	0.9395	34.02 ± 8.05	0.9265	4.00	0.25
5b	4-CH3	155.70 ± 17.11	0.9842	233.50 ± 17.73	0.9796	45.91 ± 6.15	0.9682	0.67	1.50
5c	4-OCH3	110.60 ± 15.69	0.9706	250.10 ± 31.80	0.9310	102.00 ± 8.75	0.9869	0.44	2.26
5d	4-Br	85.53 ± 9.41	0.9807	39.64 ± 7.64	0.9440	99.33 ± 17.95	0.9435	2.16	0.46
5e	3-Br	202.00 ± 23.26	0.9655	79.63 ± 14.18	0.9550	34.46 ± 5.78	0.9496	2.54	0.39
5f	4-Cl	95.83 ± 16.88	0.9572	74.76 ± 10.76	0.9742	35.58 ± 7.09	0.9355	1.28	0.78
5g	3-Cl	119.10 ± 16.35	0.9726	78.93 ± 12.44	0.9636	50.87 ± 11.66	0.9243	1.51	0.66
5h	4-F	66.60 ± 6.58	0.9860	127.30 ± 26.75	0.9337	93.74 ± 19.97	0.9255	0.52	1.91
5i	2-Cl,6-F	93.14 ± 15.34	0.9580	136.70 ± 20.99	0.9753	61.39 ± 7.94	0.9721	0.68	1.47
5j	2-Cl,4-F	111.50 ± 17.72	0.9690	106.80 ± 20.25	0.9607	41.69 ± 4.40	0.9790	1.04	0.96
5k	4-CN	260.50 ± 32.36	0.9376	152.60 ± 28.75	0.9602	154.50 ± 16.66	0.9820	1.71	0.59
5l	4-NO_2	68.63 ± 7.06	0.9848	74.94 ± 11.63	0.9664	30.95 ± 2.78	0.9856	0.92	1.09
AAZ[e]	–	439.17 ± 9.30	0.9990	98.28 ± 1.69	0.9992	–	–	–	–
THA[f]	–	–	–	–	–	159.61 ± 8.41	0.9899	–	–

[a]Human carbonic anhydrase I.
[b]Human carbonic anhydrase II.
[c]Acetylcholinesterase.
[d]Selectivity index of inhibitors for cytosolic *h*CA II over target isoform *h*CA I, calculated as the ratio of K_I off-target *h*CA/K_I target *h*CA. A potent, selective inhibitor is characterized by a high-value ratio.
[e]Acetazolamide.
[f]Tacrine.

Table 4. Antiproliferative activities of the selected beta-lactam substituted benzenesulfonamides against human breast cancer (MCF-7) cell line with the IC_{50} values and inhibition percentages.

Compounds ID	IC_{50} (μM)	Inhibition%
5d	>100	62.12
5f	38.25 ± 0.08	69.62
5g	ND[a]	68.94
5h	46.98 ± 0.13	57.61
5i	70.57 ± 0.04	45.45
5l	31.99 ± 0.14	62.05

[a]Non-determined.

278.40 nM, respectively) recorded the least inhibiting activity in the series. Exploring the inhibitory activity of novel synthesized beta-lactam substituted benzenesulfonamides (**5a-l**), all molecules showed potent inhibitory action towards the physiologically dominant *h*CA II isoform with K_Is ranging from 39.64 to 250.10 nM, which is even better than the standard drug AAZ (K_I of 98.28 nM). In particular, 4-bromo derivative **5d** exhibited the best *h*CA II inhibitory activity with K_I of 39.64 nM, whereas **5b**,**c** and **5h–k** exerted the least activity with three-digit K_Is ranging between 106.80 and 250.10 nM. All the synthesized beta-lactam substituted benzenesulfonamide derivatives (**5a–l**) strongly inhibited the AChE, with two to three-digit K_Is of 30.95–154.50 nM compared to standard drug THA (K_I of 159.61 nM). The 4-nitro substituted **5 l** derivative showed the most robust inhibitory effect with K_I of 30.95 nM. Also, unsubstituted **5a** (K_I of 34.02 nM) displayed a similar activity to both the 3-bromo **5e** and 4-chloro **5f** derivatives (K_Is of 34.46 nM and 35.58 nM, respectively). Also, 4-metoxy **5c** and 4-cyano **5k** derivatives had the weakest AChE inhibitory activity with three-digit nanomolar K_Is of 102.00 nM and 154.50 nM, respectively.

Regarding SAR, the presence of the electron-withdrawing groups, 3- to 4-chlorophenyl (**5g** and **5f**), 3- to 4-bromophenyl (**5e** and **5d**), 4-fluorophenyl (**5h**), 2-chloro-4-fluorophenyl (**5j**), 2-chloro-6-fluorophenyl (**5i**), 4-cyanophenyl (**5k**), and 4-nitrophenyl (**5 l**) derivatives or the electron-donating groups, 4-methyphenyl (**5b**) and 4-methoxyphenyl (**5c**) resulted in an increase of affinity against the cytosolic isoform *h*CA I when compared to the unsubstituted phenyl (**5a**, K_I of 278.40 nM). In particular, derivatives **5h**, **5l**, and **5d**, having 4-fluorophenyl, 4-nitrophenyl, and 4-bromophenyl moiety with K_Is of 66.60, 68.63 and 85.53 nM, respectively, were found to be 4.18, 4.06 and 3.26 times more effective than its **5a**. Substituting phenyl ring with 4-bromide (**5d**, K_I of 39.64 nM) resulted in the highest activity against *h*CA II isoform, whereas, the presence of electron-donating groups such as methyl and methoxy significantly led to decreased activity versus this isoform. On the other hand, replacing at the 4-position bromide moiety (**5d**) with a chloride or fluoride group decreased the inhibitory activity against *h*CA II by 1.89 and 3.21 times, as seen in the **5f** and **5h**, respectively (K_Is of 74.76 nM and 127.30 nM). Substituting phenyl ring with halogens such as 3-bromo **5e** with K_I of 34.46 nM and 4-chloride **5f** with K_I of 35.58 nM resulted in a little reduction of activity against AChE. But, the decline of the K_I constant (i.e. increased inhibitory activity towards AChE) was observed when the substituting phenyl ring with 4-nitro was as in **5l** (K_I of 30.95 nM).

The *h*CAs have a high degree of similarity in their primary sequences, with over 30% sequence identity. This makes it

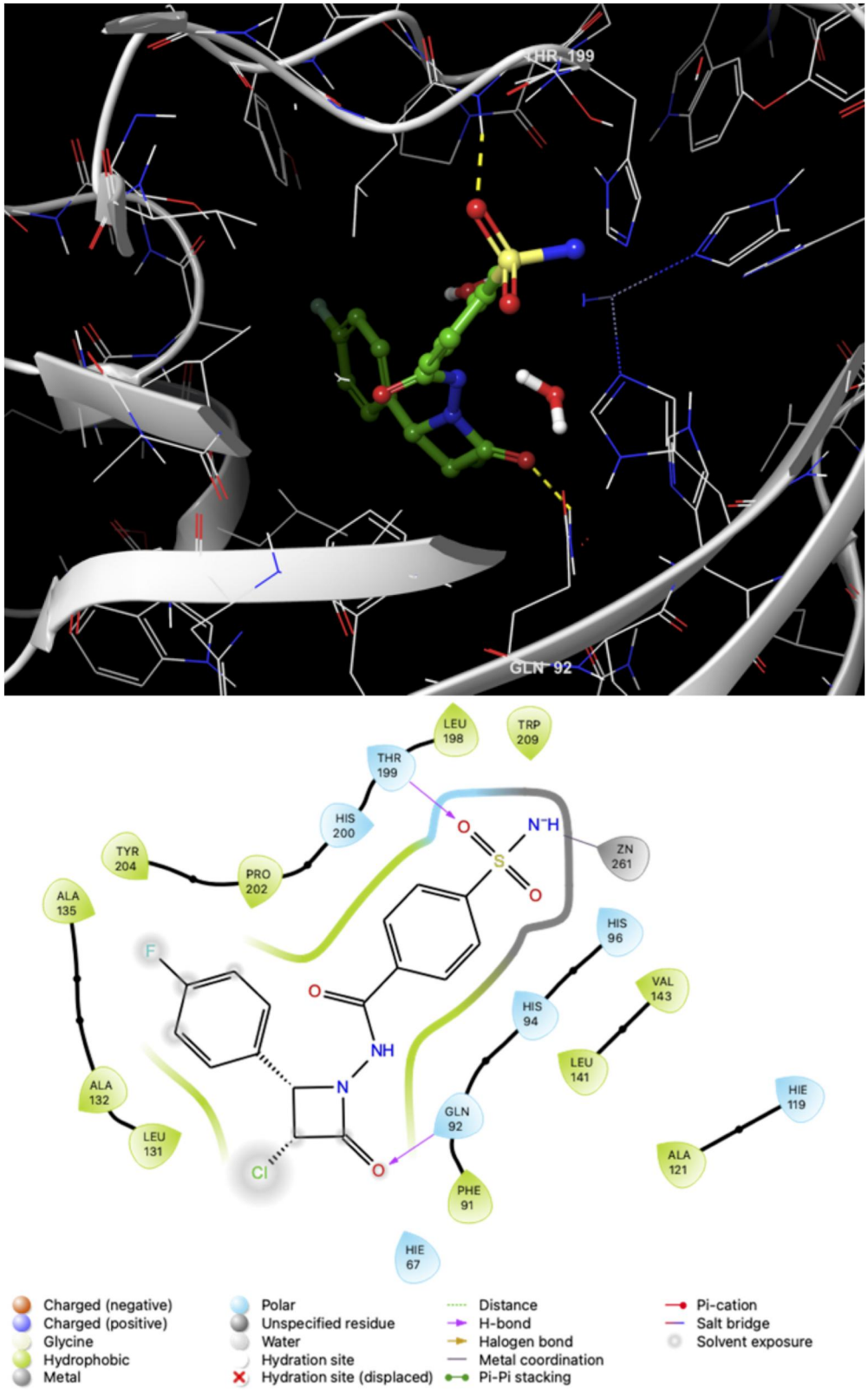

Figure 2. The binding of compound **5h** (*N*-(3-chloro-2-(4-fluorophenyl)-4-oxoazetidin-1-yl)-4-sulfamoylbenzamide) with *h*CA I isoform (PDB ID 1AZM) was explored through molecular docking. The interacting amino acids are shown in the figures, which include both 3D (top) and 2D (bottom) images that are synchronized for clarity.

difficult to design isoform-selective *h*CAIs, as many of the residues that are conserved across the isoforms are located in the active site. However, the novel beta-lactam substituted benzenesulfonamide derivatives (**5a–l**) developed in this study exhibit notable selectivity for the target isoform *h*CA II over the off-target isoform *h*CA I. The selectivity index (S_I), calculated as the ratio of the K_I for *h*CA I to the K_I for *h*CA II, was used to measure enzyme selectivity (see Table 3). The

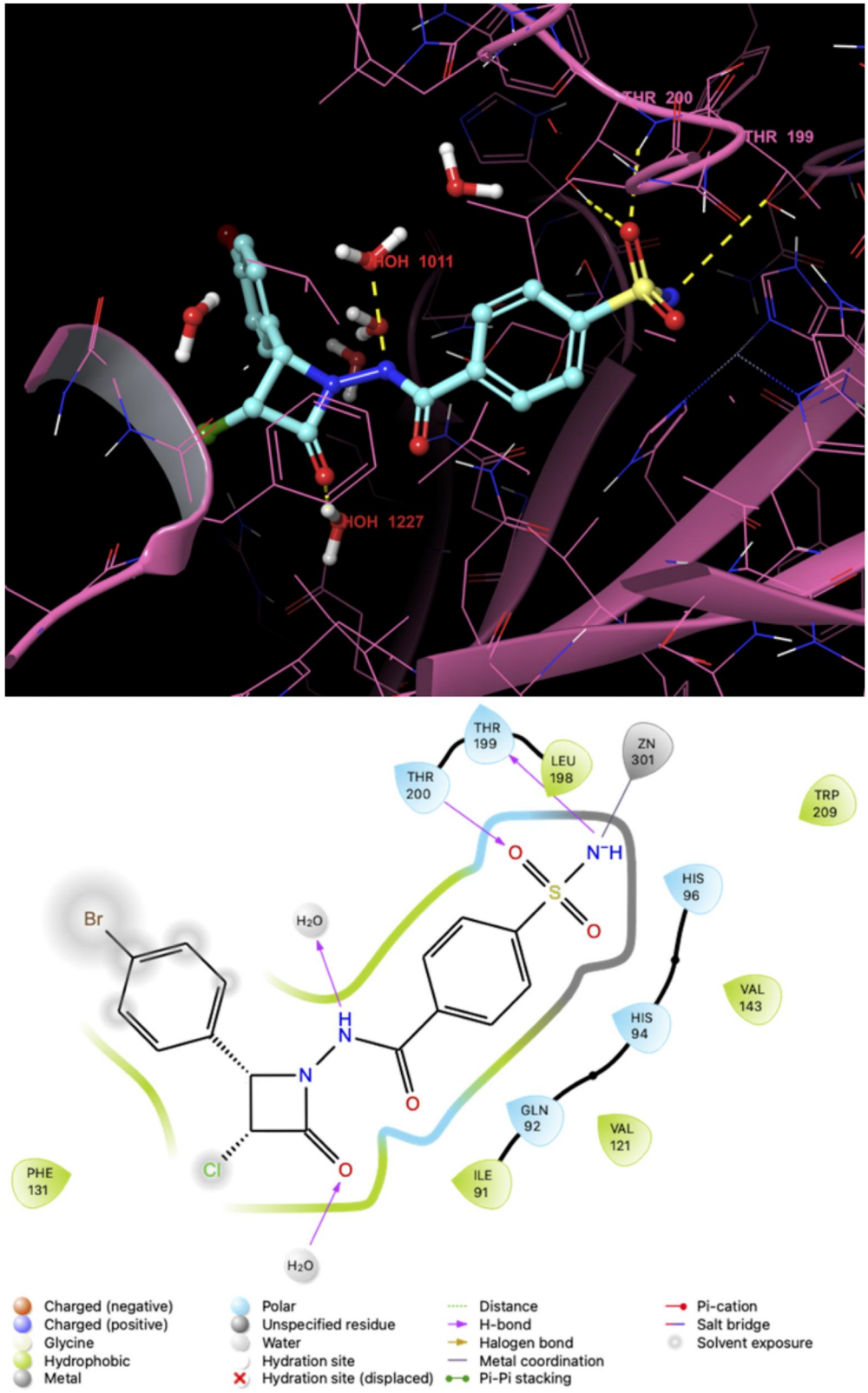

Figure 3. The binding of compound **5d** (*N*-(2-(4-bromophenyl)-3-chloro-4-oxoazetydin-1-yl)-4-sulfamoylbenzamide) with *h*CA II isoform (PDB ID 3HS4) was explored through molecular docking. The interacting amino acids are shown in the figures, which include both 3D (top) and 2D (bottom) images that are synchronized for clarity.

S_Is for the beta-lactam substituted benzenesulfonamides (**5a-l**) ranged from 4.00 to 0.44, with the unsubstituted derivative **5a** showing the highest selectivity towards *h*CA II (S_I of 4.00). The presence of electron-donating groups such as 4-methyl (**5b**) or 4-methoxy (**5c**) significantly reduced the selectivity (S_Is of 0.67 and 0.44, respectively). On the other hand, the presence of strong electron-withdrawing groups such as 4-chloro (**5d**), 3-chloro (**5e**), 3-bromo (**5f**) and 4-bromo (**5g**)

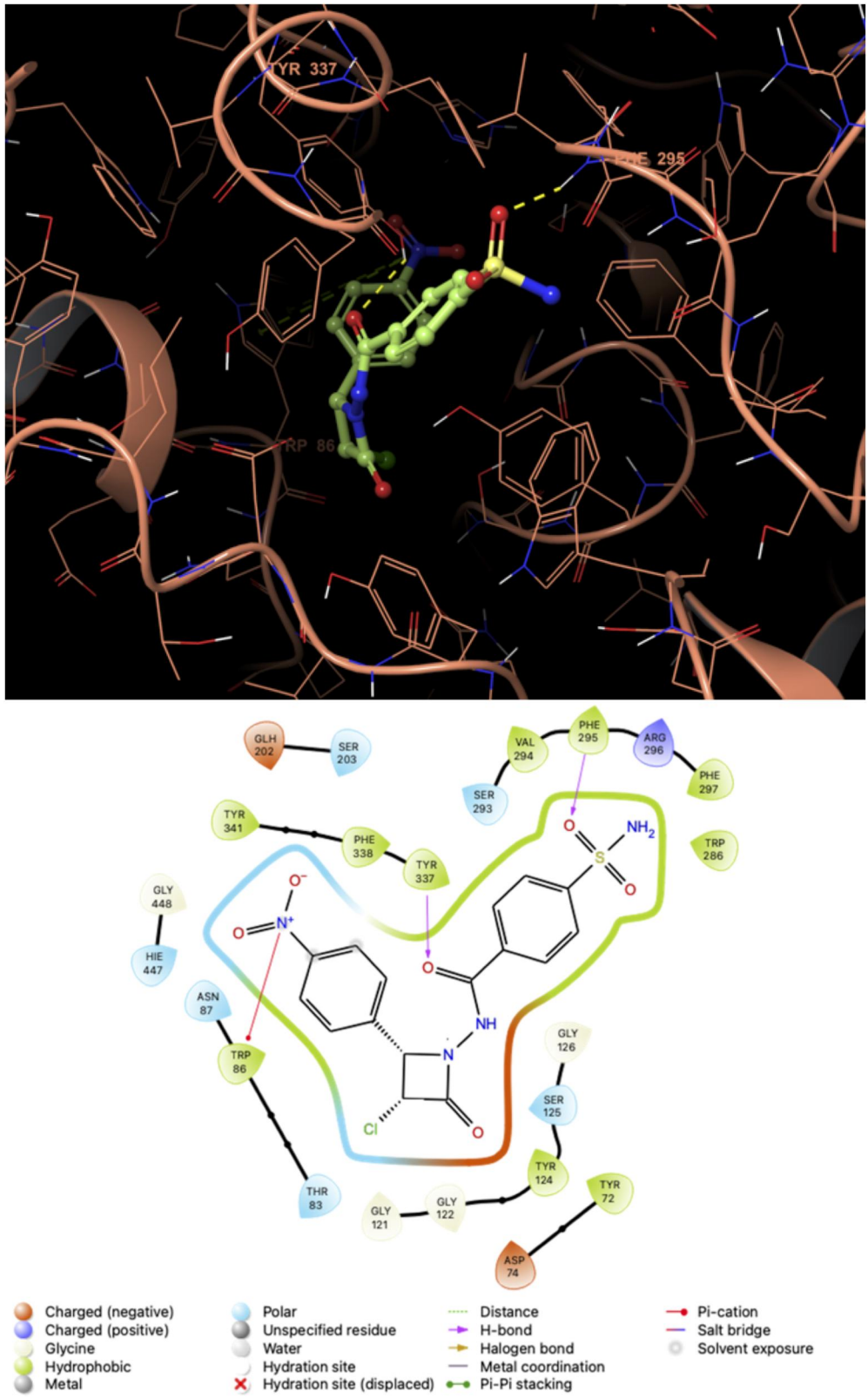

Figure 4. The binding of compound **5l** (*N*-(3-chloro-2-(4-nitrophenyl)-4-oxoazetidin-1-yl)-4-sulfamoylbenzamide) with AChE (PDB ID 7E3I) was explored through molecular docking. The interacting amino acids are shown in the figures, which include both 3D (top) and 2D (bottom) images that are synchronized for clarity.

had a negative impact on selectivity, with S_Is of 2.16, 2.54, 1.28 and 1.51, respectively. Replacing these halogen groups at the 4 position with a fluoro group in **5h** also decreased the selectivity (S_Is of 1.27 and 1.14, respectively).

3.3. Cytotoxic activity of the target compounds

Based on *in vitro* enzymatic assays, selected beta-lactam substituted benzenesulfonamides (**5d**, **5f**–**5i** and **5l**) were screened for their cytotoxic activity against the human breast

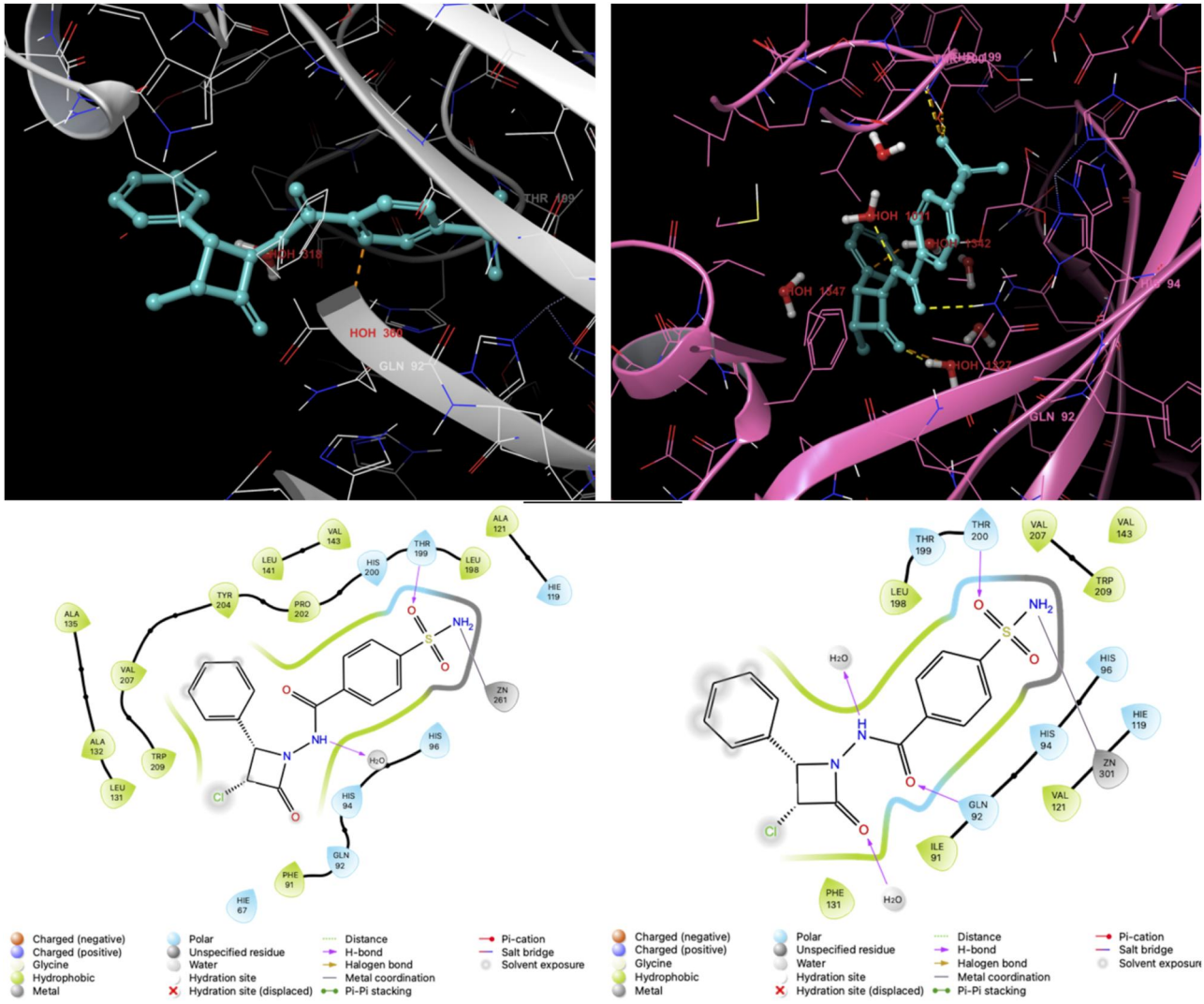

Figure 5. A comparison of the 3D and 2D binding modes of the *h*CA I isoform (PDB ID 1AZM) complexed with compound **5a** (*N*-(3-chloro-2-oxo-4-phenylazetydin-1-yl)-4-sulfamoylbenzamide) and the *h*CA II isoform (PDB ID 3HS4) complexed with compound **5a** is shown. The left image displays the *h*CA I isoform complex, while the right image displays the *h*CA II isoform complex. The interacting amino acids are shown in the figures, which include both 3D (top) and 2D (bottom) images that are synchronized for clarity.

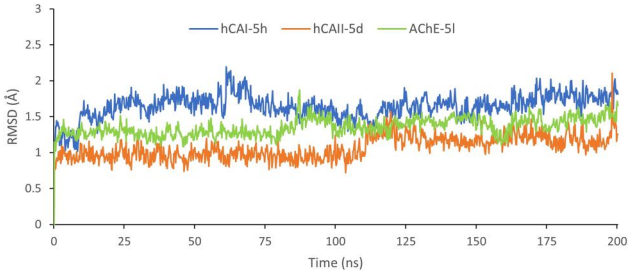

Figure 6. Protein RMSD plots as a function of simulation time.

cancer (MCF-7) cell line using the MTT assay protocol. Table 4 summarizes all tested compounds' IC_{50} and growth inhibition% values. Among them, compounds **5f**, **5h** and **5l** displayed the best inhibitory effect against MCF-7 cells with IC_{50} values of 38.3, 47.0 and 32.0 μM, respectively. Against MCF-7 cells, the IC_{50} values of cisplatin as 53 μM (Pasaribu et al., 2021), 5-fluorouracil as >100 μM (Long et al., 2019), 95.6 μM, and 1057.6 μM (Alqahtani et al., 2022) were determined based on the reference drugs in the previous research. In particular, the **5f** and **5l** were at least two to three times more potent than 5-fluorouracil and almost one time more potent than cisplatin in the MCF-7 cell line. This result means that the compounds exhibit much stronger anticancer activities than cisplatin and 5-fluorouracil. The **5f**, **5h** and **5l** showed percentage growth inhibition in the range of 57.61-69.62%. As a result, **5f** exhibited the highest cytotoxic activity with higher inhibition and low IC_{50} value (69.62% and 38.25 μM), followed by **5l** and **5h**. The results suggested that the **5f**, **5h** and **5l** were the most potential hits for further research.

3.4. In silico study

The binding patterns of the newly synthesized beta-lactam substituted benzenesulfonamides (**5a–l**) were examined using X-ray crystallographic structures of *h*CA I (PDB code 1AZM), *h*CA II (PDB code 3HS4), and AChE (PDB code 7E3I). The native ligands AZM (5-acetamido-1,3,4-thiadiazole-2-sulfonamide) and THA (1,2,3,4-tetrahydro-9-acridinamine) were

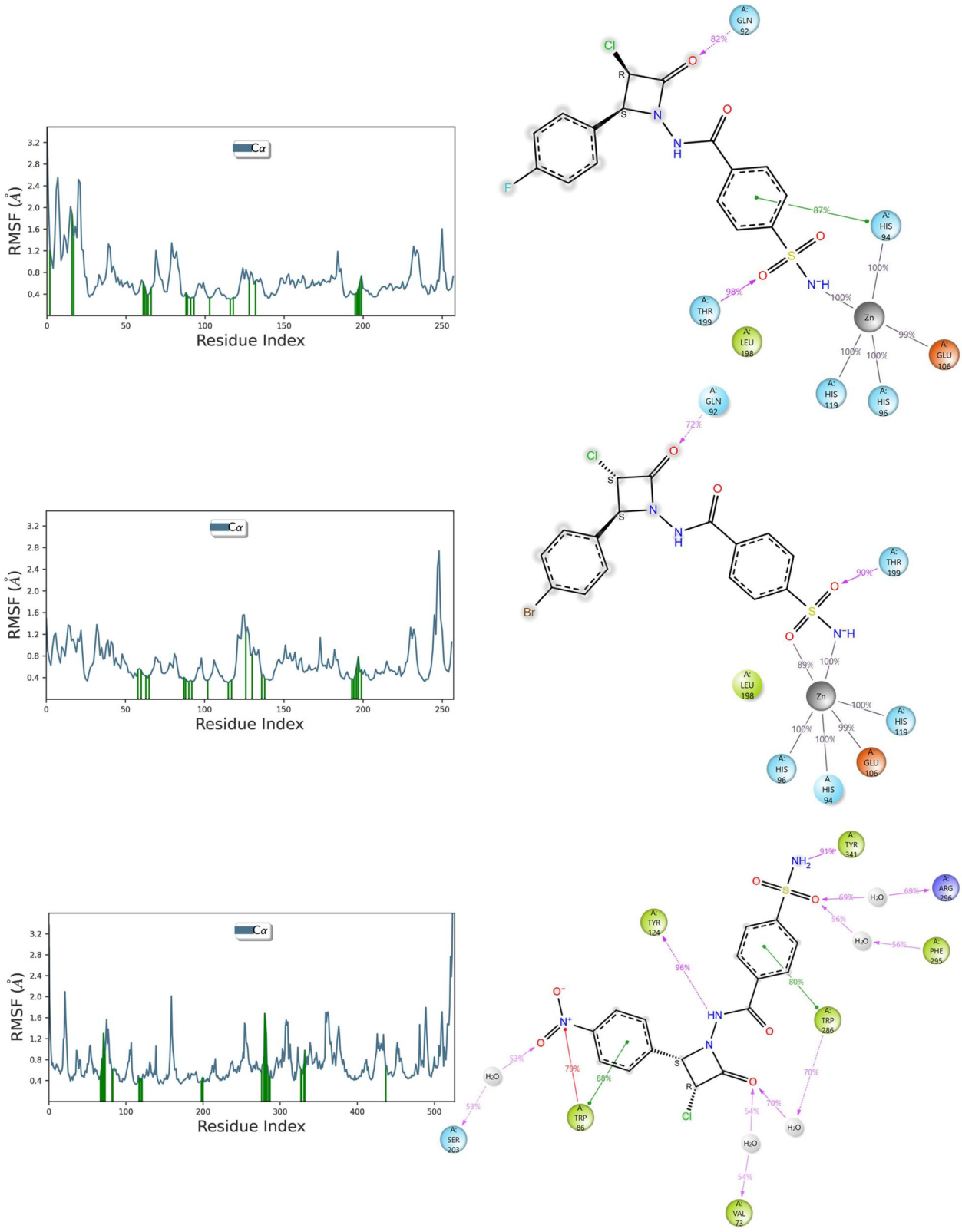

Figure 7. Protein RMSF plots as a function of amino acid residues and 2D ligand protein contacts throughout MD simulations (top: *h*CAI-**5h**, Middle *h*CAII-**5d** and bottom AChE-**5l**).

re-docked in the enzyme binding sites to confirm the validity of the docking setup. The minimal RMSD values (0.34, 1.20, and 0.26 Å, respectively) and the ability of the docking poses of the co-crystalized ligands to reproduce essential interactions demonstrated the viability of the used docking methodology. The binding mechanisms of the newly synthesized benzenesulfonamides in these *h*CAs and AChE active sites were subsequently examined using the validated setup.

The most potent inhibitors, **5h**, **5d** and **5l**, exhibited strong binding affinity to *h*CA I, *h*CA II and AChE,

Table 5. ADME/T related parameters[a] of novel synthesized beta-lactam substituted benzenesulfonamides **5a–l** and the reference inhibitors acetazolamide and tacrine, the clinically used drugs.

Compounds ID	CNS	MW	Dipole	Volume	donorHB	acceptHB	QPlogPoct	QPlogPw	QPlogPo/w	QPlogS	QPPCaco	QPlogBB	QPlogKp	Metab	QPlogKhsa	HOA	PSA	Rule of Five	Rule of Three	PAINS
5a	−2	379.82	10.41	1075.41	2.25	8.25	22.14	15.31	1.38	−4.23	48.93	−1.90	−4.63	2	−0.18	65.27	135.60	0	0	0
5b	−2	393.84	6.67	1134.13	2.25	8.25	21.81	15.01	1.65	−4.74	48.52	−1.98	−4.84	2	−0.05	66.79	135.63	0	0	0
5c	−2	409.84	10.97	1152.84	2.25	9.00	23.12	15.56	1.48	−4.51	48.78	−2.05	−4.73	2	−0.18	65.82	143.62	0	0	0
5d	−2	458.71	4.42	1126.81	2.25	8.25	21.83	15.08	1.91	−5.02	48.37	−1.78	−4.82	1	−0.07	68.29	135.67	0	0	0
5e	−2	458.71	10.22	1129.09	2.25	8.25	22.89	15.09	1.93	−5.06	48.50	−1.79	−4.81	2	−0.06	68.39	135.63	0	0	0
5f	−2	414.26	9.32	1119.73	2.25	8.25	22.54	15.07	1.85	−4.92	48.75	−1.78	−4.81	1	−0.08	68.01	135.63	0	0	0
5g	−2	414.26	10.25	1119.51	2.25	8.25	22.76	15.08	1.85	−4.94	48.67	−1.79	−4.80	2	−0.08	67.98	135.63	0	0	0
5h	−2	397.81	9.09	1091.41	2.25	8.25	22.06	15.13	1.61	−4.64	48.86	−1.84	−4.75	1	−0.15	66.58	135.27	0	0	0
5i	−2	432.25	7.29	1118.09	2.25	8.25	22.13	15.02	1.86	−4.76	49.90	−1.70	−4.80	2	−0.07	68.23	134.04	0	0	0
5j	−2	432.25	8.70	1121.66	2.25	8.25	22.48	14.91	1.95	−4.98	48.93	−1.67	−4.88	1	−0.07	68.63	135.21	0	0	0
5k	−2	404.83	2.00	1140.07	2.25	9.75	22.40	16.95	0.64	−5.29	10.25	−2.82	−5.96	1	−0.34	48.77	161.09	0	1	0
5l	−2	424.82	2.37	1147.92	2.25	9.25	22.28	16.44	0.67	−4.40	5.80	−3.03	−6.54	2	−0.23	44.54	180.58	0	1	0
AAZ [b]	−2	222.24	10.76	634.43	3.00	9.00	17.57	15.15	−1.75	−1.55	36.88	−1.74	−5.90	1	−0.97	44.77	134.97	0	0	0
THA [c]	1	198.27	4.22	710.28	1.50	2.00	10.75	6.38	2.59	−3.14	2931.00	0.04	−1.78	3	0.07	100.00	34.21	0	0	0

[a]CNS, Central nervous system activity (−2 inactive and +2 active); MW, molecular weight of the compound (130.00–725.00); Dipole, computed dipole moment of the compound (1.00–12.50); Volume, total solvent-accessible volume in cubic angstroms using a probe with a 1.4 A° Radius (500.00–2000.00); donorHB, estimated number of hydrogen bonds that would be donated by the solute to water molecules in an aqueous solution (0–6); acceptHB, estimated number of hydrogen bonds that would be accepted by the solute from water molecules in an aqueous solution (2–20); QPlogPoct, octanol/gas partition coefficient (8.00–35.00); QPlogPw, water/gas partition coefficient (4.00–45.00); QPlogPo/w, octanol/water partition coefficient (−2.00 to 6.50); QPlogS, aqueous solubility (−6.50 to 0.50); QPPCaco, apparent Caco-2 cell permeability in nm/sec (<25 poor, great > 500); QPlogBB, brain/blood partition coefficient (−3.00 to 1.20); QPlogKp, skin permeability (−8.00 to −1.00); Metab, number of likely metabolic reactions (1–8); QPlogKhsa, prediction of binding to human serum albumin (−1.50 to 1.50); HOA; human oral absorption (<25% poor, high > 80%); PSA, van der Waals surface area of polar nitrogen and oxygen atoms (7.00–200.00); Rule of Five, number of violations of Lipinski's rule of five (max. 4); Rule of Three, number of violations of Jorgensen's rule of three (max. 3); PAINS, pan-assay interference compounds alert.
[b]Acetazolamide.
[c]Tacrine.

respectively, with K_Is of 66.6, 39.6 and 31.0 nM, respectively. These inhibitors demonstrated predicted binding scores of −7.50 kcal/mol and MM-GBSA value of −24.20 kcal/mol in *h*CA I, a docking score of −7.11 kcal/mol and MM-GBSA value of −5.95 kcal/mol in *h*CA II, and a docking score of −8.20 kcal/mol and MM-GBSA value of −49.87 kcal/mol in AChE. Compounds **5h** and **5d** displayed similar binding patterns in *h*CAs, which included the positioning of the sulfonamide moiety in the active site and interaction with the active site Zn^{2+} ions as well as hydrogen bonding with the gatekeeper residues Thr199 (1.86 Å distance for *h*CA I and 2.60 Å distance for *h*CA II) and Thr200 (2.02 Å distance for *h*CA II). The beta-lactam ring engaged in a hydrogen bond with the polar residue Gln92 in *h*CA I (2.30 Å distance) and a water molecule in *h*CA II (1.69 Å distance). In *h*CA II, a hydrogen bond interaction also occurred between the amide moiety of **5d** and a water molecule (1.88 Å distance). Compound **5l** and AChE formed a hydrogen bond interaction between the oxygen atom of the benzenesulfonamide moiety and Phe295 residue (1.77 Å distance). Additionally, the hydrophobic residue Tyr337 (2.30 Å distance) formed a hydrogen bond with the carboxy moiety, while the nitro moiety exhibited a π-cation interaction with Trp86 (Figures 2–4).

The binding of compound **5a** to the *h*CA II isoform exhibits notable selectivity, as indicated by the selectivity index of 4.00. This selectivity may be attributed to the interactions of **5a** with the gatekeeper residue Thr200 and other residues, such as Gln92 and water molecules (distances of 2.15, 2.28, 1.60 and 1.69 Å), in the *h*CA II binding pocket. In contrast, in the *h*CA I binding pocket, **5a** primarily interacts with Thr199 (distance of 2.06 Å) and a water molecule (distance of 1.90 Å) through hydrogen bonding. These specific interactions in the *h*CA II binding pocket may allow for a stronger binding of **5a** to this isoform. It is worth noting that the hydrogen bonds and distances between **5a** and *h*CA II are important for the observed selectivity. These unique binding characteristics may enable **5a** to fit more securely in the *h*CA II binding cavity (Figure 5).

The docked conformers of the potent compounds **5h**, **5d** and **5l** were subjected to MD simulations to assess the stability of the enzyme–ligand complexes under physiological conditions and also, to confirm the interaction profiles of the ligands with vital amino acid residues at the molecular level as a function of simulation time. In all three cases, the RMSD plots shown in Figure 6 indicate a stable binding interaction with slight deviations from the initial position that remained within an acceptable thermal average of 1–3 Å.

The RMSFs were used to depict the fluctuations of each residue present in enzymes over the simulation time (Figure 7). Although there seem to be a few high fluctuations, most of the amino acid fluctuations were less than 1.2 Å. Green vertical lines in Figure 7 represent ligand contacts. Low fluctuations were observed for most of the residues with which the ligands interact, which can be concluded that the interactions are quite stable. On the other hand, some fluctuations of the ligands were observed in each case. Inspection of the 200 ns trajectories revealed that the mainly aromatic ring bonded to the beta-lactam was flexible

during the course of the simulation resulting in minor conformational changes throughout the simulation. However, the ligands were still remaining in the binding pocket.

To see how long the ligand–amino acid interactions were stable during the simulation time, ligand-protein contacts were also evaluated (Figure 7). Contacts that were observed for 50% of the course of the simulations were evaluated. In addition to water bridges, the interaction of compound **5h** with Zn metal in *h*CAI remained for 100% of the time, while hydrogen bonds between Thr199 and Gln92 were also stable for 98% and 82% of the simulation, respectively. A π interaction was also observed with His94 residue. In the *h*CAII-**5d** system, the critical metallic interaction with Zn was also conserved for 100% of the simulation time, and also hydrogen bond with Gln92 was formed over 70% of the time. In the MD study of AChE complex, during at least 80% of the time, compound **5l** interacted mainly with the peripheral anionic site (Thy41, Tyr124 and Trp286) and anionic site (Trp86) of AChE.

Additionally, the novel synthesized beta-lactam substituted benzenesulfonamides (**5a–l**) were evaluated for their drug-like properties using the QikProp module of the Schrödinger Suite 2022-3 for Mac. The selected ADME/T parameters were computed and listed in Table 5. These results showed that, based on their physicochemical characteristics, the derivatives **5a–l** met the criteria for drug-like molecules as defined by Lipinski's (Lipinski et al., 1997) and Jorgensen's (Duffy & Jorgensen, 2000) rules.

4. Conclusion

In the present study, we designed, synthesized, and evaluated the inhibitory effects of twelve beta-lactam-substituted benzenesulfonamides (**5a–l**) on the *h*CA I, II isoforms, and AChE. These new inhibitors contained benzenesulfonamide as a ZBG motif, linked to a phenyl tail through a beta-lactam linker. The SAR analysis showed that substitution of the phenyl tail with unsubstituted phenyl (**5a**, K_I of 69.6 nM), bromo (**5d** and **5e**, K_Is of 39.6 nM and 79.6 nM, respectively), chloro (**5f** and **5g**, K_Is of 74.8 nM and 78.9 nM, respectively), and nitro (**5 l**, K_I of 75.0 nM) groups conferred potent *h*CA II inhibitory activity. Notably, the unsubstituted sulfanilamide derivative **5a** selectively inhibited *h*CA II isoform with a selectivity of $>$ 4-fold over *h*CA I. On the other hand, all derivatives (**5a–l**) incorporating both electron-donating and electron-withdrawing groups exhibited effective *h*CA I and AChE inhibitory activity. In addition, selected beta-lactam substituted benzenesulfonamides were screened for their cytotoxic activity against the MCF-7 cell line using the MTT assay protocol. Compounds **5f** and **5l** showed promising anticancer activities, with IC_{50} values of 38.3 μM and 32.0 μM, respectively, after 24 h of treatment, which were more potent than 5-fluorouracil and cisplatin against the MCF-7 cell line. Moreover, molecular docking was used to investigate the binding of the sulfonamide moiety of the beta-lactam substituted benzenesulfonamides to the active sites of *h*CAs and AChE. The results suggested that these compounds fit well into the active sites of these enzymes and interact with the Zn^{2+} ions present *h*CAs. The MD simulations revealed significant stability of each enzyme-ligand complex during 200 ns and confirmed favorable interactions with the crucial amino acid residues in the binding pocket. Also, it is determined that these compounds under investigation displayed drug-like traits based on physicochemical properties, and all the derivatives (**5a–l**) comply with Lipinski's and Jorgensen's rules. These results suggest that the reported derivatives have the potential to be exploited in the design of novel, next-generation inhibitors, based on the insights of the inhibition data in terms of SARs.

Disclosure statement

No potential conflict of interest was reported by the authors.

Acknowledgements

Author Özcan Güleç is a 100/2000 The Council of Higher Education (CoHE) Ph.D. Scholar in the Organic Smart and Innovative Materials Subsection.

Funding

This work was supported by the Research Fund of Sakarya University (grant number 2021-7-24-56), the Research Fund of Erzincan Binali Yıldırım University (grant number TSA-2020-729), and the Research Fund of Anadolu University (grant number 2102S003).

ORCID

Özcan Güleç http://orcid.org/0000-0002-4803-845X
Cüneyt Türkeş http://orcid.org/0000-0002-2932-2789
Mustafa Arslan http://orcid.org/0000-0003-0796-4374
Yeliz Demir http://orcid.org/0000-0001-8320-8517
Busra Dincer http://orcid.org/0000-0002-3365-7741
Abdulilah Ece http://orcid.org/0000-0002-3087-5145
Şükrü Beydemir http://orcid.org/0000-0003-3667-6902

Data availability statement

Data will be made available on request. All spectra that support the characterization of the compounds is provided in the Supporting Information.

References

Aggarwal, M., Boone, C. D., Kondeti, B., & McKenna, R. (2013). Structural annotation of human carbonic anhydrases. *Journal of Enzyme Inhibition and Medicinal Chemistry*, *28*(2), 267–277. https://doi.org/10.3109/14756366.2012.737323

Alım, Z., Tunç, T., Demirel, N., Günel, A., & Karacan, N. (2022). Synthesis of benzimidazole derivatives containing amide bond and biological evaluation as acetylcholinesterase, carbonic anhydrase I and II inhibitors. *Journal of Molecular Structure*, *1268*, 133647. https://doi.org/10.1016/j.molstruc.2022.133647

Alqahtani, A. S., Ghorab, M. M., Nasr, F. A., Ahmed, M. Z., Al-Mishari, A. A., & Attia, S. M. (2022). Novel sulphonamide-bearing methoxyquinazolinone derivatives as anticancer and apoptosis inducers: Synthesis, biological evaluation and in silico studies. *Journal of Enzyme Inhibition and Medicinal Chemistry*, *37*(1), 86–99. https://doi.org/10.1080/14756366.2021.1983807

Alterio, V., Di Fiore, A., D'Ambrosio, K., Supuran, C. T., & De Simone, G. (2012). Multiple binding modes of ınhibitors to carbonic anhydrases: How to design specific drugs targeting 15 different ısoforms? *Chemical Reviews*, *112*(8), 4421–4468. https://doi.org/10.1021/cr200176r

Arya, N., Dwivedi, J., Khedkar, V. M., Coutinho, E. C., & Jain, K. S. (2013). Design, synthesis and biological evaluation of some 2-azetidinone derivatives as potential antihyperlipidemic agents. *Archiv der Pharmazie*, *346*(12), 872–881. https://doi.org/10.1002/ardp.201300262

Askin, S., Tahtaci, H., Türkeş, C., Demir, Y., Ece, A., Çiftçi, G. A., & Beydemir, Ş. (2021). Design, synthesis, characterization, in vitro and in silico evaluation of novel imidazo [2, 1-b][1, 3, 4] thiadiazoles as highly potent acetylcholinesterase and non-classical carbonic anhydrase inhibitors, Bioorg. *Bioorganic Chemistry*, *113*, 105009. https://doi.org/10.1016/j.bioorg.2021.105009

Atmaca, U., Aksoy, M., & Öztekin, A. (2022). A safe alternative synthesis of primary carbamates from alcohols; in vitro and in silico assessments as an alternative acetylcholinesterase inhibitors. *Journal of Biomolecular Structure & Dynamics*, 1–10. https://doi.org/10.1080/07391102.2022.2134209

Barreiro, G., Guimarães, C. R. W., Tubert-Brohman, I., Lyons, T. M., Tirado-Rives, J., & Jorgensen, W. L. (2007). Search for non-nucleoside ınhibitors of HIV-1 reverse transcriptase using chemical similarity, molecular docking, and MM-GB/SA scoring. *Journal of Chemical İnformation and Modeling*, *47*(6), 2416–2428. https://doi.org/10.1021/ci700271z

Bekku, S., Mochizuki, H., Yamamoto, T., Ueno, H., Takayama, E., & Tadakuma, T. (2000). Expression of carbonic anhydrase I or II and correlation to clinical aspects of colorectal cancer. *Hepato-gastroenterology*, *47*(34), 998–1001.

Bonardi, A., Nocentini, A., Bua, S., Combs, J., Lomelino, C., Andring, J., Lucarini, L., Sgambellone, S., Masini, E., McKenna, R., Gratteri, P., & Supuran, C. T. (2020). Sulfonamide ınhibitors of human carbonic anhydrases designed through a three-tails approach: Improving ligand/ısoform matching and selectivity of action. *Journal of Medicinal Chemistry*, *63*(13), 7422–7444. https://doi.org/10.1021/acs.jmedchem.0c00733

Bowers, K. J., Chow, E., Xu, H., Dror, R. O., Eastwood, M. P., Gregersen, B. A., Klepeis, J. L., Kolossvary, I., Moraes, M. A., & Sacerdoti, F. D. (2006). *Scalable algorithms for molecular dynamics simulations on commodity clusters* [Paper presentation]. Proceedings of the 2006 ACM/IEEE Conference on Supercomputing, pp. 84-es. https://doi.org/10.1145/1188455.1188544

Bozdag, M., Ferraroni, M., Nuti, E., Vullo, D., Rossello, A., Carta, F., Scozzafava, A., & Supuran, C. T. (2014). Combining the tail and the ring approaches for obtaining potent and isoform-selective carbonic anhydrase inhibitors: Solution and X-ray crystallographic studies. *Bioorganic & Medicinal Chemistry*, *22*(1), 334–340. https://doi.org/10.1016/j.bmc.2013.11.016

Brandi, A., Cicchi, S., & Cordero, F. M. (2008). Novel syntheses of azetidines and azetidinones. *Chemical Reviews*, *108*(9), 3988–4035. https://doi.org/10.1021/cr800325e

Buza, A., Türkeş, C., Arslan, M., Demir, Y., Dincer, B., Nixha, A. R., & Beydemir, Ş. (2023). Discovery of novel benzenesulfonamides incorporating 1,2,3-triazole scaffold as carbonic anhydrase I, II, IX, and XII inhibitors. *International Journal of Biological Macromolecules*, *239*, 124232. https://doi.org/10.1016/j.ijbiomac.2023.124232

Carosso, S., & Miller, M. J. (2015). Syntheses and studies of new forms of N-sulfonyloxy β-lactams as potential antibacterial agents and β-lactamase inhibitors. *Bioorganic & Medicinal Chemistry*, *23*(18), 6138–6147. https://doi.org/10.1016/j.bmc.2015.08.005

Carta, F., Aggarwal, M., Maresca, A., Scozzafava, A., McKenna, R., Masini, E., & Supuran, C. T. (2012). Dithiocarbamates strongly ınhibit carbonic anhydrases and show antiglaucoma action in vivo. *Journal of Medicinal Chemistry*, *55*(4), 1721–1730. https://doi.org/10.1021/jm300031j

Chakravarty, S., & Kannan, K. K. (1994). Drug-protein ınteractions: Refined structures of three sulfonamide drug complexes of human carbonic anhydrase I enzyme. *Journal of Molecular Biology*, *243*(2), 298–309. https://doi.org/10.1006/jmbi.1994.1655

Cheung, J., Rudolph, M. J., Burshteyn, F., Cassidy, M. S., Gary, E. N., Love, J., Franklin, M. C., & Height, J. J. (2012). Structures of human acetylcholinesterase in complex with pharmacologically ımportant ligands. *Journal of Medicinal Chemistry*, *55*(22), 10282–10286. https://doi.org/10.1021/jm300871x

Daryadel, S., Atmaca, U., Taslimi, P., Gülçin, İ., & Çelik, M. (2018). Novel sulfamate derivatives of menthol: Synthesis, characterization, and cholinesterases and carbonic anhydrase enzymes inhibition properties. *Archiv Der Pharmazie*, *351*(11), 1800209. https://doi.org/10.1002/ardp.201800209

Demir, Y., Türkes¸, C., C¸avus¸, M. S., Erdoğan, M., Muğlu, H., Yakan, H., & Beydemir, S. (2023). Enzyme inhibition, molecular docking, and DFT studies of new thiosemicarbazones incorporating 4-hydroxy-3,5-dimethoxy benzaldehyde motif. *Archiv der Pharmazie (Weinheim, Ger.)*, *356*(4), 202200554. https://doi.org/10.1002/ardp.202200554

Duffy, E. M., & Jorgensen, W. L. (2000). Prediction of properties from simulations: Free energies of solvation in hexadecane, octanol, and water. *Journal of the American Chemical Society*, *122*(12), 2878–2888. https://doi.org/10.1021/ja993663t

Ece, A. (2020). Towards more effective acetylcholinesterase inhibitors: A comprehensive modelling study based on human acetylcholinesterase protein–drug complex. *Journal of Biomolecular Structure & Dynamics*, *38*(2), 565–572. https://doi.org/10.1080/07391102.2019.1583606

Elbadawi, M. M., Eldehna, W. M., Nocentini, A., Abo-Ashour, M. F., Elkaeed, E. B., Abdelgawad, M. A., Alharbi, K. S., Abdel-Aziz, H. A., Supuran, C. T., Gratteri, P., & Al-Sanea, M. M. (2021). Identification of N-phenyl-2-(phenylsulfonyl)acetamides/propanamides as new SLC-0111 analogues: Synthesis and evaluation of the carbonic anhydrase inhibitory activities. *European Journal of Medicinal Chemistry*, *218*, 113360. https://doi.org/10.1016/j.ejmech.2021.113360

Elbadawi, M. M., Eldehna, W. M., Nocentini, A., Somaa, W. R., Al-Rashood, S. T., Elkaeed, E. B., El Hassab, M. A., Abdel-Aziz, H. A., Supuran, C. T., & Fares, M. (2022). Development of 4-((3-oxo-3-phenylpropyl)amino)-benzenesulfonamide derivatives utilizing tail/dual-tail approaches as novel carbonic anhydrase inhibitors. *European Journal of Medicinal Chemistry*, *238*, 114412. https://doi.org/10.1016/j.ejmech.2022.114412

Eldeeb, A. H., Abo-Ashour, M. F., Angeli, A., Bonardi, A., Lasheen, D. S., Elrazaz, E. Z., Nocentini, A., Gratteri, P., Abdel-Aziz, H. A., & Supuran, C. T. (2021). Novel benzenesulfonamides aryl and arylsulfone conjugates adopting tail/dual tail approaches: Synthesis, carbonic anhydrase inhibitory activity and molecular modeling studies. *European Journal of Medicinal Chemistry*, *221*, 113486. https://doi.org/10.1016/j.ejmech.2021.113486

Ellman, G. L., Courtney, K. D., Andres, V., & Feather-Stone, R. M. (1961). A new and rapid colorimetric determination of acetylcholinesterase activity. *Biochemical Pharmacology*, *7*(2), 88–95. 5, https://doi.org/10.1016/0006-2952(61)90145-9

Fisher, S. Z., Maupin, C. M., Budayova-Spano, M., Govindasamy, L., Tu, C., Agbandje-McKenna, M., Silverman, D. N., Voth, G. A., & McKenna, R. (2007). Atomic crystal and molecular dynamics simulation structures of human carbonic anhydrase II: Insights into the proton transfer mechanism. *Biochemistry*, *46*(11), 2930–2937. https://doi.org/10.1021/bi062066y

Friesner, R. A., Banks, J. L., Murphy, R. B., Halgren, T. A., Klicic, J. J., Mainz, D. T., Repasky, M. P., Knoll, E. H., Shelley, M., Perry, J. K., Shaw, D. E., Francis, P., & Shenkin, P. S. (2004). Glide: A new approach for rapid, accurate docking and scoring. 1. Method and assessment of docking accuracy. *Journal of Medicinal Chemistry*, *47*(7), 1739–1749. https://doi.org/10.1021/jm0306430

Gök, N., Akıncıoğlu, A., Erümit Binici, E., Akıncıoğlu, H., Kılınç, N., & Göksu, S. (2021). Synthesis of novel sulfonamides with anti-Alzheimer and antioxidant capacities. *Archiv der Pharmazie*, *354*(7), 2000496. https://doi.org/10.1002/ardp.202000496

Güleç, Ö., Türkeş, C., Arslan, M., Demir, Y., Yeni, Y., Hacımüftüoğlu, A., Ereminsoy, E., Küfrevioğlu, Ö. İ., & Beydemir, Ş. (2022). Cytotoxic effect, enzyme inhibition, and in silico studies of some novel N-substituted sulfonyl amides incorporating 1,3,4-oxadiazol structural motif. *Molecular Diversity*, *26*(5), 2825–2845. https://doi.org/10.1007/s11030-022-10422-8

Güller, P., Dağalan, Z., Güller, U., Çalışır, U., & Nişancı, B. (2021). Enzymes inhibition profiles and antibacterial activities of benzylidenemalononitrile derivatives. *Journal of Molecular Structure*. *1239*, 130498. https://doi.org/10.1016/j.molstruc.2021.130498

Güngör, S. A., Köse, M., Tümer, M., Türkeş, C., & Beydemir, Ş. (2022). Synthesis, characterization and docking studies of benzenesulfonamide derivatives containing 1,2,3-triazole as potential ınhibitor of carbonic anhydrase I-II enzymes. *Journal of Biomolecular Structure & Dynamics*, 1–11. https://doi.org/10.1080/07391102.2022.2159531

Halgren, T. A. (2009). Identifying and characterizing binding sites and assessing druggability. *Journal of Chemical İnformation and Modeling*, *49*(2), 377–389. https://doi.org/10.1021/ci800324m

Halgren, T. A., Murphy, R. B., Friesner, R. A., Beard, H. S., Frye, L. L., Pollard, W. T., & Banks, J. L. (2004). Glide: A new approach for rapid, accurate docking and scoring. 2. Enrichment factors in database screening. *Journal of Medicinal Chemistry*, *47*(7), 1750–1759. https://doi.org/10.1021/jm030644s

Kakakhan, C., Türkeş, C., Güleç, Ö., Demir, Y., Arslan, M., Özkemahlı, G., & Beydemir, Ş. (2023). Exploration of 1,2,3-triazole linked benzenesulfonamide derivatives as isoform selective inhibitors of human carbonic anhydrase. *Bioorganic & Medicinal Chemistry*, *77*, 117111. https://doi.org/10.1016/j.bmc.2022.117111

Karakılıç, E., Alım, Z., Günel, A., & Baran, A. (2022). A versatile study of novel A3B-type unsymmetric zinc(II) phthalocyanines containing thiazolidin-4-one: Their, carbonic anhydrase I, II isoenzymes, and xanthine oxidase inhibitors evaluation. *Journal of Molecular Structure*, *1257*, 132630. https://doi.org/10.1016/j.molstruc.2022.132630

Kılıcaslan, S., Arslan, M., Ruya, Z., Bilen, Ç., Ergün, A., Gençer, N., & Arslan, O. (2016). Synthesis and evaluation of sulfonamide-bearing thiazole as carbonic anhydrase isoforms hCA I and hCA II. *Journal of Enzyme İnhibition and Medicinal Chemistry*, *31*(6), 1300–1305. https://doi.org/10.3109/14756366.2015.1128426

Kim, J.-H., Cho, S. Y., Lee, J.-H., Jeong, S. M., Yoon, I.-S., Lee, B.-H., Lee, J.-H., Pyo, M. K., Lee, S.-M., Chung, J.-M., Kim, S., Rhim, H., Oh, J.-W., & Nah, S.-Y. (2007). Neuroprotective effects of ginsenoside Rg3 against homocysteine-induced excitotoxicity in rat hippocampus. *Brain Research*, *1136*(1), 190–199. https://doi.org/10.1016/j.brainres.2006.12.047

Kumar, A., Siwach, K., Supuran, C. T., & Sharma, P. K. (2022). A decade of tail-approach based design of selective as well as potent tumor associated carbonic anhydrase inhibitors. *Bioorganic Chemistry*, *126*, 105920. https://doi.org/10.1016/j.bioorg.2022.105920

Kumar, K., Singh, P., Kremer, L., Guérardel, Y., Biot, C., & Kumar, V. (2012). Synthesis and in vitro anti-tubercular evaluation of 1,2,3-triazole tethered β-lactam–ferrocene and β-lactam–ferrocenylchalcone chimeric scaffolds. *Dalton Transactions (Cambridge, England: 2003)*, *41*(19), 5778–5781. https://doi.org/10.1039/C2DT30514C

Kuskovsky, R., Lloyd, D., Arora, K., Plotkin, B. J., Green, J. M., Boshoff, H. I., Barry, C., Deschamps, J., & Konaklieva, M. I. (2019). C4-Phenylthio β-lactams: Effect of the chirality of the β-lactam ring on antimicrobial activity. *Bioorganic & Medicinal Chemistry*, *27*(20), 115050. https://doi.org/10.1016/j.bmc.2019.115050

Lankat-Buttgereit, B., Gregel, C., Knolle, A., Hasilik, A., Arnold, R., & Göke, R. (2004). Pdcd4 inhibits growth of tumor cells by suppression of carbonic anhydrase type II. *Molecular and Cellular Endocrinology*, *214*(1-2), 149–153. https://doi.org/10.1016/j.mce.2003.10.058

Leitans, J., Kazaks, A., Balode, A., Ivanova, J., Zalubovskis, R., Supuran, C. T., & Tars, K. (2015). Efficient expression and crystallization system of cancer-associated carbonic anhydrase ısoform IX. *Journal of Medicinal Chemistry*, *58*(22), 9004–9009. https://doi.org/10.1021/acs.jmedchem.5b01343

Lipinski, C. A., Lombardo, F., Dominy, B. W., & Feeney, P. J. (1997). Experimental and computational approaches to estimate solubility and permeability in drug discovery and development settings. *Advanced Drug Delivery Reviews*. *23*(1-3), 3–25. https://doi.org/10.1016/S0169-409X(96)00423-1

Lolak, N., Akocak, S., Durgun, M., Duran, H. E., Necip, A., Türkeş, C., Işık, M., & Beydemir, Ş. (2022). Novel bis-ureido-substituted sulfaguanidines and sulfisoxazoles as carbonic anhydrase and acetylcholinesterase inhibitors. *Molecular Diversity*. https://doi.org/10.1007/s11030-022-10527-0

Long, X-k., Liao, L.-Q., Zeng, Y.-F., Zhang, Y., Xiao, F., Li, C., & Guo, Y. (2019). Synthesis and biological evaluation of novel genistein amino acid ester derivatives as potential anti-tumor agents. *ChemistrySelect*, *4*(19), 5662–5666. https://doi.org/10.1002/slct.201900857

Madhavi Sastry, G., Adzhigirey, M., Day, T., Annabhimoju, R., & Sherman, W. (2013). Protein and ligand preparation: Parameters, protocols, and influence on virtual screening enrichments. *Journal of Computer-Aided Molecular Design*, *27*(3), 221–234. https://doi.org/10.1007/s10822-013-9644-8

Malebari, A. M., Fayne, D., Nathwani, S. M., O'Connell, F., Noorani, S., Twamley, B., O'Boyle, N. M., O'Sullivan, J., Zisterer, D. M., & Meegan, M. J. (2020). β-Lactams with antiproliferative and antiapoptotic activity in breast and chemoresistant colon cancer cells. *European Journal of Medicinal Chemistry*, *189*(2020), 112050. https://doi.org/10.1016/j.ejmech.2020.112050

Mehta, P. D., Sengar, N. P. S., & Pathak, A. K. (2010). 2-Azetidinone – A new profile of various pharmacological activities. *European Journal of Medicinal Chemistry*, *45*(12), 5541–5560. https://doi.org/10.1016/j.ejmech.2010.09.035

Michaelis, L., Menten, M. L., Johnson, K. A., & Goody, R. S. (2011). The Original Michaelis Constant: Translation of the 1913 Michaelis–Menten Paper. *Biochemistry*, *50*(39), 8264–8269. https://doi.org/10.1021/bi201284u

Mishra, C. B., Kumari, S., Angeli, A., Bua, S., Mongre, R. K., Tiwari, M., & Supuran, C. T. (2021). Discovery of potent carbonic anhydrase ınhibitors as effective anticonvulsant agents: Drug design, synthesis, and ın vitro and ın vivo ınvestigations. *Journal of Medicinal Chemistry*, *64*(6), 3100–3114. https://doi.org/10.1021/acs.jmedchem.0c01889

Mishra, C. B., Kumari, S., Angeli, A., Monti, S. M., Buonanno, M., Tiwari, M., & Supuran, C. T. (2017). Discovery of benzenesulfonamides with potent human carbonic anhydrase ınhibitory and effective anticonvulsant action: Design, synthesis, and pharmacological assessment. *Journal of Medicinal Chemistry*, *60*(6), 2456–2469. https://doi.org/10.1021/acs.jmedchem.6b01804

Mishra, C. B., Tiwari, M., & Supuran, C. T. (2020). Progress in the development of human carbonic anhydrase inhibitors and their pharmacological applications: Where are we today? *Medicinal Research Reviews*, *40*(6), 2485–2565. https://doi.org/10.1002/med.21713

Nocentini, A., & Supuran, C. T. (2019). Advances in the structural annotation of human carbonic anhydrases and impact on future drug discovery. *Expert Opinion on Drug Discovery*, *14*(11), 1175–1197. https://doi.org/10.1080/17460441.2019.1651289

Osazee, J. O. (2016). Molecular docking, synthesis and evaluation of pyrrolo [2, 1-c][1, 4] benzodiazepines derivatives as non-β-lactam β-lactamases ınhibitors. East Tennessee State University.

Osmaniye, D., Türkeş, C., Demir, Y., Özkay, Y., Beydemir, Ş., & Kaplancıklı, Z. A. (2022). Design, synthesis, and biological activity of novel dithiocarbamate-methylsulfonyl hybrides as carbonic anhydrase inhibitors. *Archiv der Pharmazie*, *355*(8), e2200132. https://doi.org/10.1002/ardp.202200132

Ozer, E. B., Caglayan, C., & Bayindir, S. (2022). The solvent-controlled regioselective synthesis of 3-amino-5-aryl-rhodanines as novel inhibitors of human carbonic anhydrase enzymes. *Tetrahedron*, *120*, 132896. https://doi.org/10.1016/j.tet.2022.132896

Page, M. I. (1987). The mechanisms of reactions of β-lactam antibiotics. In: D. Bethell (Ed.), *Advances in physical organic chemistry* (pp. 165–270). Academic Press.

Parkkila, S., Lasota, J., Fletcher, J. A., Ou, W-b., Kivelä, A. J., Nuorva, K., Parkkila, A.-K., Ollikainen, J., Sly, W. S., Waheed, A., Pastorekova, S., Pastorek, J., Isola, J., & Miettinen, M. (2010). Carbonic anhydrase II. A novel biomarker for gastrointestinal stromal tumors. *Modern Pathology : An Official Journal of the United States and Canadian Academy of Pathology, Inc*, *23*(5), 743–750. https://doi.org/10.1038/modpathol.2009.189

Pasaribu, Y. P., Fadlan, A., Fatmawati, S., & Ersam, T. (2021). Biological activity evaluation and ın silico studies of polyprenylated benzophenones from *Garcinia celebica*. *Biomed*, *9*(11), 1654. https://doi.org/10.3390/biomedicines9111654

Rad, J. A., Jarrahpour, A., Latour, C., Sinou, V., Brunel, J. M., Zgou, H., Mabkhot, Y., Hadda, T. B., & Turos, E. (2017). Synthesis and

antimicrobial/antimalarial activities of novel naphthalimido trans-β-lactam derivatives. *Medicinal Chemistry Research*, *26*(10), 2235–2242. https://doi.org/10.1007/s00044-017-1920-z

Ramírez Granillo, A., Canales, M. G. M., Espíndola, M. E. S., Martínez Rivera, M. A., de Lucio, V. M. B., & Tovar, A. V. R. (2015). Antibiosis interaction of Staphylococccus aureus on Aspergillus fumigatus assessed in vitro by mixed biofilm formation. *BMC Microbiology*, *15*(1), 33. https://doi.org/10.1186/s12866-015-0363-2

Sahoo, B. M., & Banik, B. K. (2020). Therapeutic potentials of β-lactam. In *Synthetic approaches to nonaromatic nitrogen heterocycles* (pp. 59–88). Wiley.

Saturnino, C., Fusco, B., Saturnino, P., Martino, G. D. E., Rocco, F., & Lancelot, J.-C. (2000). Evaluation of analgesic and anti-inflammatory activity of novel β-lactam monocyclic compounds. *Biological & Pharmaceutical Bulletin*, *23*(5), 654–656. https://doi.org/10.1248/bpb.23.654

Schrödinger release 2023-1: Desmond. (2023). Schrödinger, LLC.

Schrödinger release 2023-1: Epik. (2023). Schrödinger, LLC.

Schrödinger release 2023-1: Glide. (2023). Schrödinger, LLC.

Schrödinger release 2023-1: LigPrep. (2023). Schrödinger, LLC.

Schrödinger release 2023-1: Prime. (2023). Schrödinger, LLC.

Schrödinger release 2023-1: Protein preparation wizard. (2023). Schrödinger, LLC.

Schrödinger release 2023-1: QikProp. (2023). Schrödinger, LLC.

Schrödinger release 2023-1: Receptor grid generation. (2023). Schrödinger, LLC.

Schrödinger release 2023-1: SiteMap. (2023). Schrödinger, LLC.

Scozzafava, A., & Supuran, C. T. (2014). Glaucoma and the applications of carbonic anhydrase ınhibitors. In: S.C. Frost & R. McKenna (Eds.), *Carbonic anhydrase: Mechanism, regulation, links to disease, and ındustrial applications* (pp. 349–359). Springer Netherlands.

Sever, B., Türkeş, C., Altıntop, M. D., Demir, Y., Çiftçi, G. A., & Beydemir, Ş. (2021). Novel metabolic enzyme inhibitors designed through the molecular hybridization of thiazole and pyrazoline scaffolds. *Archiv Der Pharmazie*, *354*(12), e2100294. https://doi.org/10.1002/ardp.202100294

Shelley, J. C., Cholleti, A., Frye, L. L., Greenwood, J. R., Timlin, M. R., & Uchimaya, M. (2007). Epik: A software program for pKaprediction and protonation state generation for drug-like molecules. *Journal of Computer-Aided Molecular Design*, *21*(12), 681–691. https://doi.org/10.1007/s10822-007-9133-z

Singh, G. S. (2004a). β-Lactams in the new millennium. Part-I: Monobactams and carbapenems. *Mini - Reviews in Medicinal Chemistry*, *4*(1), 69–92. https://doi.org/10.2174/1389557043487501

Singh, G. S. (2004b). β-lactams in the new millennium. Part-II: Cephems, oxacephems, penams and sulbactam. *Mini - Reviews in Medicinal Chemistry*, *4*(1), 93–109. https://doi.org/10.2174/1389557043487547

Singh, H., Vasa, S. K., Jangra, H., Rovó, P., Päslack, C., Das, C. K., Zipse, H., Schäfer, L. V., & Linser, R. (2019). Fast microsecond dynamics of the protein–water network in the active site of human carbonic anhydrase II studied by solid-state NMR spectroscopy. *Journal of the American Chemical Society*, *141*(49), 19276–19288. https://doi.org/10.1021/jacs.9b05311

Sippel, K. H., Robbins, A. H., Domsic, J., Genis, C., Agbandje-McKenna, M., & McKenna, R. (2009). High-resolution structure of human carbonic anhydrase II complexed with acetazolamide reveals insights into inhibitor drug design. *Acta Crystallographica. Section F, Structural Biology and Crystallization Communications*, *65*(Pt 10), 992–995. https://doi.org/10.1107/S1744309109036665

Sperka, T., Pitlik, J., Bagossi, P., & Tözsér, J. (2005). Beta-lactam compounds as apparently uncompetitive inhibitors of HIV-1 protease. *Bioorganic & Medicinal Chemistry Letters*, *15*(12), 3086–3090. https://doi.org/10.1016/j.bmcl.2005.04.020

Supuran, C. T. (2018). Applications of carbonic anhydrases inhibitors in renal and central nervous system diseases. *Expert Opinion on Therapeutic Patents*, *28*(10), 713–721. https://doi.org/10.1080/13543776.2018.1519023

Taslimi, P., Türkan, F., Cetin, A., Burhan, H., Karaman, M., Bildirici, I., Gulçin, İ., & Şen, F. (2019). Pyrazole[3,4-d]pyridazine derivatives: Molecular docking and explore of acetylcholinesterase and carbonic anhydrase enzymes inhibitors as anticholinergics potentials, Bioorg. *Bioorganic Chemistry*, *92*, 103213. https://doi.org/10.1016/j.bioorg.2019.103213

Tawfik, H. O., Petreni, A., Supuran, C. T., & El-Hamamsy, M. H. (2022). Discovery of new carbonic anhydrase IX inhibitors as anticancer agents by toning the hydrophobic and hydrophilic rims of the active site to encounter the dual-tail approach. *European Journal of Medicinal Chemistry*, *232*, 114190. https://doi.org/10.1016/j.ejmech.2022.114190

Topal, F. (2019). Inhibition profiles of voriconazole against acetylcholinesterase, α-glycosidase, and human carbonic anhydrase I and II isoenzymes. *Journal of Biochemical and Molecular Toxicology*, *33*(10), e22385. https://doi.org/10.1002/jbt.22385

Türkeş, C., Arslan, M., Demir, Y., Cocaj, L., Nixha, A. R., & Beydemir, Ş. (2019). Synthesis, biological evaluation and in silico studies of novel N-substituted phthalazine sulfonamide compounds as potent carbonic anhydrase and acetylcholinesterase inhibitors, Bioorg. *Bioorganic Chemistry*, *89*, 103004. https://doi.org/10.1016/j.bioorg.2019.103004

Türkeş, C., Demir, Y., & Beydemir, Ş. (2021). Calcium channel blockers: molecular docking and ınhibition studies on carbonic anhydrase I and II ısoenzymes. *Journal of Biomolecular Structure & Dynamics*, *39*(5), 1672–1680. https://doi.org/10.1080/07391102.2020.1736631

Veinberg, G., Shestakova, I., Vorona, M., Kanepe, I., & Lukevics, E. (2004). Synthesis of antitumor 6-alkylidenepenicillanate sulfones and related 3-alkylidene-2-azetidinones. *Bioorganic & Medicinal Chemistry Letters*, *14*(1), 147–150. https://doi.org/10.1016/j.bmcl.2003.09.078

Verpoorte, J. A., Mehta, S., & Edsall, J. T. (1967). Esterase activities of human carbonic anhydrases B and C. *Journal of Biological Chemistry*, *242*(18), 4221–4229. https://doi.org/10.1016/S0021-9258(18)95800-X

Vigorita, M. G., Ottanà, R., Monforte, F., Maccari, R., Trovato, A., Monforte, M. T., & Taviano, M. F. (2001). Synthesis and antiinflammatory, analgesic activity of 3,3′-(1,2-Ethanediyl)-bis[2-aryl-4-thiazolidinone] chiral compounds. Part 10. *Bioorganic & Medicinal Chemistry Letters*, *11*(21), 2791–2794. https://doi.org/10.1016/S0960-894X(01)00476-0

Wang, S., Bao, L., Song, D., Wang, J., & Cao, X. (2019). Heterocyclic lactam derivatives containing piperonyl moiety as potential antifungal agents. *Bioorganic & Medicinal Chemistry Letters*, *29*(20), 126661. https://doi.org/10.1016/j.bmcl.2019.126661

Yakan, H., Muğlu, H., Türkeş, C., Demir, Y., Erdoğan, M., Çavuş, M. S., & Beydemir, Ş. (2023). A novel series of thiosemicarbazone hybrid scaffolds: Design, synthesis, DFT studies, metabolic enzyme inhibition properties, and molecular docking calculations. *Journal of Molecular Structure*, *1280*, 135077. https://doi.org/10.1016/j.molstruc.2023.135077

Yapar, G., Duran, H. E., Lolak, N., Akocak, S., Türkeş, C., Durgun, M., Işık, M., & Beydemir, Ş. (2021). Biological effects of bis-hydrazone compounds bearing isovanillin moiety on the aldose reductase. *Bioorganic Chemistry*, *117*, 105473. https://doi.org/10.1016/j.bioorg.2021.105473

Yararli, K., Ozer, E. B., Bayindir, S., Caglayan, C., Turkes, C., & Beydemir, S. (2023). The synthesis, biological evaluation and in silico studies of asymmetric 3,5-diaryl-rhodanines as novel inhibitors of human carbonic anhydrase isoenzymes. *Journal of Molecular Structure*. *1276*, 134783. https://doi.org/10.1016/j.molstruc.2022.134783

Zhang, X., & Jia, Y. (2020). Recent advances in β-lactam derivatives as potential anticancer agents. *Current Topics in Medicinal Chemistry*, *20*(16), 1468–1480. https://doi.org/10.2174/1568026620666620030916144

Zhang, X., Hubbard, C. D., & van Eldik, R. (1996). Carbonic anhydrase catalysis: A volume profile analysis. *The Journal of Physical Chemistry*, *100*(21), 9161–9171. https://doi.org/10.1021/jp9524791